Electronic supplementary information

Robust silver-mediated imidazolo-dC base pairs in metal DNA: dinuclear silver bridges with exceptional stability in double helices with parallel and antiparallel strand orientation

Sunit Kumar Jana,[a] Xiurong Guo,[a,c] Hui Mei,[a] and Frank Seela*[a,b]

[a]*Laboratory of Bioorganic Chemistry and Chemical Biology, Center for Nanotechnology, Heisenbergstraße 11, 48149 Münster, Germany*

[b] *Laboratorium für Organische und Bioorganische Chemie, Institut für Chemie neuer Materialien, Universität Osnabrück, Barbarastraße 7, 49069 Osnabrück, Germany*

[c]*Institute for Nanobiomedical Technology and Membrane Biology, West China Medicinal School, No. 1 Keyuan 4th Road, Gaopengdadao, Chengdu 610041, P.R. China*

Corresponding author: Prof. Dr. Frank Seela

Phone: +49 (0) 251 53406 500; Fax: +49 (0) 251 53406 857

E-mail: Frank.Seela@uni-osnabrueck.de

Homepage: www.seela.net

Contents

General methods and materials.

All chemicals and solvents were of laboratory grade as obtained from commercial suppliers and were used without further purification. Thin-layer chromatography (TLC) was performed on TLC aluminium sheets covered with silica gel 60 F254. Flash column chromatography (FC): silica gel 60 at 0.4 bar. UV-spectra: U-3200 UV-vis spectrometer. ^{1}H, ^{13}C and ^{31}P NMR spectra were measured at 300.15 MHz for ^{1}H, 75.48 MHz for ^{13}C, and 121.52 MHz for ^{31}P. δ values in ppm rel. to Me_4Si as internal standard (^{1}H and ^{13}C) or external 85% H_3PO_4 (^{31}P). The *J* values are given in Hz. For NMR spectra measured in DMSO-d_6, the chemical shift of the solvent peak was set to 2.50 ppm for ^{1}H-NMR and 39.50 ppm for ^{13}C-NMR. DEPT-135 and ^{1}H-^{13}C gated-decoupled spectra were used for the assignment of the ^{13}C signals (Table S1). For ^{1}H-^{13}C coupling constants see Table S2. Reversed-phase HPLC was carried out on a 4 × 250 mm RP-18 (10 µm) LiChrospher 100 column with a HPLC pump connected with a variable wavelength monitor, a controller and an integrator. The molecular masses of the oligonucleotides were determined by MALDI-TOF mass spectrometry in the linear positive mode with 3-hydroxypicolinic acid (3-HPA) as a matrix. The thermal melting curves were measured with a UV/Vis spectrophotometer equipped with a thermoelectrical controller. The temperature was measured continuously in the reference cell with a Pt-100 resistor with a heating rate of 1°C min^{-1}. The calculation of thermodynamic data was performed with the program MeltWin[1] (version 3.0) using curve fitting of the melting profiles according to a two-state model.

Synthesis, purification, and characterization of oligonucleotides.

The oligonucleotide syntheses were performed on an ABI 392-08 synthesizer at 1 µmol scale (trityl-on mode) employing the standard phosphoramidites and the modified building blocks **6** and **8** following the synthesis protocol for 3'-cyanoethyl phosphoramidites. The average coupling yield was always higher than 95%. After cleavage from the solid support, the

oligonucleotides were deprotected in 28% aq. NH_3 for 2 days at room temperature. The DMT-containing oligonucleotides were purified by reversed-phase HPLC (RP-18) with the following solvent gradient system: A: 0.1 M (Et_3NH)OAc (pH 7.0)/MeCN 95:5; B: MeCN; gradient *I*: 0-3 min 10-15% B in A, 3-15 min 15-50% B in A, 15-20 min 50-10% B in A, flow rate 0.8 mL min^{-1}. Then, the mixture was evaporated to dryness, and the residue was treated with 2.5% $Cl_2CHCOOH/CH_2Cl_2$ for 3 min at 0 °C to remove the 4,4'-dimethoxytrityl residues. The detritylated oligomers were purified by reversed-phase HPLC with the gradient *II*: 0-20 min 0-20% B in A, 20-25 min 20% B in A, 25-30 min 20-0% B in A, flow rate 0.8 mL min^{-1}. The oligomers were desalted on a short column (RP-18, silica gel) using H_2O for elution of the salt, while the oligomers were eluted with MeOH/H_2O (3:2). The purity of the oligonucleotides was confirmed by MALDI-TOF mass spectra (Table S4) and HPLC (RP-18) profiles (Figure S6). The oligonucleotides were lyophilized on a Speed Vac evaporator to yield colourless solids which were stored frozen at -24°C. The extinction coefficients ε_{260} (H_2O) of the nucleosides are: dA 15400, dG 11700, dT 8800, dC 7300, **1** 1400 (MeOH), **2** 22900 (MeOH) and **3** 12400 (MeOH). The extinction coefficients of the oligonucleotides were calculated from the sum of the extinction coefficients of the nucleoside constituents.

Experimental procedures.

1-(2-Deoxy-*β*-D-*erythro*-pentofuranosyl)-1*H*-purin-2(9*H*)-one (1).

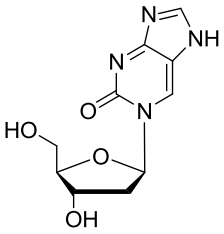

1

Compound **4**[2] (500 mg, 2.06 mmol) in diethoxymethyl acetate (5 mL) was heated at 100 °C for 3 h. Then, water (3 mL) was added and evaporated under high vacuum. The residue was purified by FC (silica gel, column 15 × 3 cm, CH_2Cl_2/MeOH, 100:15) to yield colourless solid **1** (150 mg, 0.60 mmol, 29%). TLC (silica gel, CH_2Cl_2/MeOH, 9:1): R_f 0.18. λ_{max} (MeOH)/nm 217 (ε/dm^3 mol^{-1} cm^{-1} 16900), 324 (3700).^{1}H NMR (300 MHz, DMSO-d_6): δ 1.99-2.07 (m, 1H, 2'-H), 2.31-2.39 (m, 1H, 2'-H), 3.59-3.72 (m, 2H, 2 x 5'-H), 3.88-3.89 (m, 1H, 4'-H), 4.23 (br, 1H, 3'-H), 5.23-5.26 (m, 2H, 3'-OH, 5'-OH), 6.18 (t, *J* = 6.3 Hz, 1H, 1'-H), 8.18 (s, 1H, H-8), 8.95 (s, 1H, H-6), 12.61 (br, 1H, NH). ESI-TOF: *m/z* calcd. for $C_{10}H_{12}N_4O_4$ [M + Na]$^+$ 275.0751, found 275.0750.

1-[2-Deoxy-5-*O*-(4,4'-dimethoxytriphenylmethyl)-*β*-D-*erythro*-pentofuranosyl]-1*H*-purin-2(9*H*)-one (5).

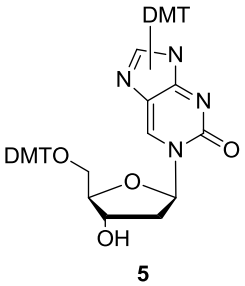

5

Compound **1** (300 mg, 1.2 mmol) was co-evaporated with pyridine (2 × 10 mL) before dissolving in pyridine (15 mL). Then, 4,4'-dimethoxytrityl chloride (950 mg, 2.88 mmol) was

added in three portions, and the reaction mixture was stirred at room temperature for 16 h. Finally, MeOH (2 mL) was added, and the mixture was stirred for another 20 min. The reaction mixture was diluted with CH_2Cl_2 (2 × 20 mL) and extracted with 5% aqueous $NaHCO_3$ solution (50 mL). The organic layer was dried over Na_2SO_4, and then concentrated. Purification by FC (silica gel, column 15 × 3 cm, CH_2Cl_2/acetone, 80:20) gave **5** as a light yellow solid (450 mg, 0.53 mmol, 44% yield). TLC (silica gel, CH_2Cl_2/acetone, 4:1): R_f 0.40. λ_{max} (MeOH)/nm 225 (ε/dm^3 mol^{-1} cm^{-1} 56100), 324 (7700). ^{1}H NMR (300 MHz, DMSO-d_6): δ 2.05-2.12 (m, 1H, 2'-H$_\alpha$), 2.31-2.37 (m, 1H, 2'-H$_\beta$), 3.17-3.29 (m, 2H, 2 x 5'-H), 3.65-3.79 (m, 12H, 4 x OCH_3), 4.00-4.01 (m, 1H, 4'-H), 4.20-4.22 (m, 1H, 3'-H), 5.31 (d, J = 4.5 Hz, 1H, 3'-OH), 6.08 (t, J = 6.0 Hz, 1H, 1'-H), 6.81-6.90 (m, 8H, DMTr-H), 7.04-7.08 (m, 4H, DMTr-H), 7.11-7.18 (m, 4H, DMTr-H), 7.21-7.31 (m, 8H, DMTr-H), 7.33-7.40 (m, 2H, DMTr-H), 7.87 (s, 1H, 8-H), 8.59 (s, 1H, 6-H). ESI-TOF: *m/z* calcd. for $C_{52}H_{48}N_4O_8$ [M + Na]$^+$ 879.3364, found 879.3371.

1-[2-Deoxy-5-*O*-(4,4'-dimethoxytriphenylmethyl)-*β*-D-*erythro*-pentofuranosyl]-1*H*-purin-2(9*H*)-one 3'-(2-cyanoethyl)-*N*,*N*'-diisopropyl phosphoramidite (6).

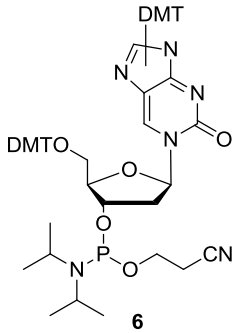

6

A stirred solution of **5** (600 mg, 0.70 mmol) in anhydrous CH_2Cl_2 (12 mL) was treated with (i-Pr)$_2$NEt (210 µL, 1.20 mmol) followed by 2-cyanoethyl-*N*,*N*-diisopropylphosphoramido-chloridite (210 µL, 0.94 mmol). After stirring for 20 min at room temperature, the solution was diluted with CH_2Cl_2 (40 mL) and extracted with 5% aq. $NaHCO_3$ solution (30 mL). The organic layer was dried over Na_2SO_4 and evaporated. The residue was purified by FC (silica

gel, column 10 x 2 cm, CH_2Cl_2/acetone, 8:1) giving **6** (215 mg, 0.20 mmol, 29% yield) as a light yellow foam. TLC (silica gel, CH_2Cl_2/acetone, 5:1): R_f 0.50. ^{31}P NMR (121 MHz, $CDCl_3$): δ 148.55, 148.97. ESI-TOF: *m/z* calcd. for $C_{61}H_{65}N_6NaO_9P$ $[M + Na]^+$ 1079.4443, found 1079.4415.

1-(2-Deoxy-*β*-D-*erythro*-pentofuranosyl)-8-furyl-1*H*-purin-2(9*H*)-one (3).

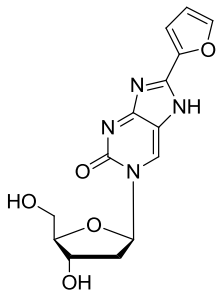

3

Furfural (108 µL, 1.3 mmol), and ceric (IV) ammonium nitrate (110 mg, 0.2 mmol) were added to a solution of 5-amino-dC **4**[2] (242 mg, 1.0 mmol) in DMF (10 mL). The solution was heated to 55 °C and stirred for 24 h. The solvent was evaporated to dryness, and the residue was purified by FC (silica gel, column 15 × 3 cm, CH_2Cl_2/MeOH, 10:1) to yield light yellow solid **3** (180 mg, 0.57 mmol, 57% yield). TLC (silica gel, CH_2Cl_2/MeOH, 5:1): R_f 0.43. λ_{max} (MeOH)/nm 274 (ε/dm^3 mol^{-1} cm^{-1} 17200), 346 (14800). ^1H NMR (300 MHz, DMSO-d_6): δ 2.03-2.11 (m, 1H, 2'-H_α), 2.32-2.40 (m, 1H, 2'-H_β), 3.60-3.74 (m, 2H, 2 x 5'-H), 3.88-3.90 (m, 1H, 4'-H), 4.24-4.25 (m, 1H, 3'-H), 5.25-5.27 (m, 2H, 3'-OH, 5'-OH), 6.21 (t, *J* = 6.1 Hz, 1H, 1'-H), 6.72-6.74 (m, 1H, furyl), 7.26-7.27 (m, 1H, furyl), 7.93-7.97 (m, 1H, furyl), 8.90 (s, 1H, 6-H), 13.10 (s, 1H, NH). ESI-TOF: *m/z* calcd. for $C_{14}H_{14}N_4O_5$ $[M + Na]^+$ 341.0856, found 341.0867.

1-[2-Deoxy-5-*O*-(4,4'-dimethoxytriphenylmethyl)-*β*-D-*erythro*-pentofuranosyl]-8-furyl-1*H*-purin-2(9*H*)-one (7).

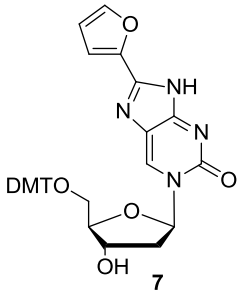

7

Compound **3** (637 mg, 2.0 mmol) was co-evaporated with pyridine (2 × 10 mL) before dissolving in pyridine (10 mL). Then, 4,4'-dimethoxytrityl chloride (879 mg, 2.60 mmol) was added in three portions, and the reaction mixture was stirred at room temperature for 16 h. Finally, MeOH (2 mL) was added, and the mixture was stirred for another 20 min. The reaction mixture was diluted with CH_2Cl_2 (2 × 20 mL) and extracted with 5% aqueous $NaHCO_3$ solution (50 mL). The organic layer was dried over Na_2SO_4, and then concentrated. Purification by FC (silica gel, column 15 × 3 cm, CH_2Cl_2/MeOH, 98:2) gave **7** as a light yellow solid (757 mg, 0.94 mmol, 47% yield). TLC (silica gel, CH_2Cl_2/MeOH, 10:1): R_f 0.48. λ_{max} (MeOH)/nm 274 (ε/dm^3 mol^{-1} cm^{-1} 19000), 252 (14400). ^{1}H NMR (300 MHz, DMSO-d_6): δ 2.12-2.21 (m, 1H, 2'-H$_\alpha$), 2.36-2.44 (m, 1H, 2'-H$_\beta$), 3.21–3.30 (m, 2H, 2 x 5'-H), 3.71 (2s, 6H, 2 x OCH_3), 4.02-4.03 (m, 1H, 4'-H), 4.18-4.22 (m, 1H, 3'-H), 5.34 (d, J = 4.2 Hz, 1H, 3'-OH), 6.24 (t, J = 6.3 Hz, 1H, 1'-H), 6.74-6.76 (m, 1H, furyl), 6.89-6.92 (m, 4H, 3 x DMTr-H, 1 x 1H, furyl), 7.19-7.42 (m, 10H, DMTr-H), 7.98-7.99 (m, 1H, furyl), 8.53 (s, 1H, 6-H), 13.13 (s, 1H, 7-NH). ESI-TOF: *m/z* calcd. for $C_{35}H_{32}N_4NaO_7$ $[M + Na]^+$ 643.2163, found 643.2166.

1-[2-Deoxy-5-*O*-(4,4'-dimethoxytriphenylmethyl)-*β*-D-*erythro*-pentofuranosyl]-8-furyl-1*H*-purin-2(9*H*)-one 3'-(2-cyanoethyl)-*N*,*N*'-diisopropyl phosphoramidite (8).

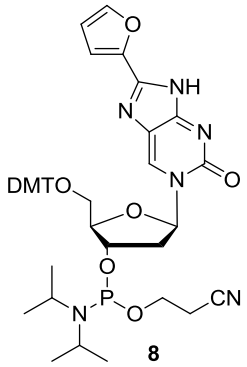

8

A stirred solution of **7** (150 mg, 0.44 mmol) in anhydrous CH_2Cl_2 (10 mL) was treated with (*i*-Pr)$_2$NEt (75 µL, 0.42 mmol) followed by 2-cyanoethyl-*N*,*N*-diisopropylphosphoramido-chloridite (67 µL, 0.3 mmol). After stirring for 10 min at room temperature, the solution was diluted with CH_2Cl_2 (40 mL) and extracted with 5% aq. $NaHCO_3$ solution (30 mL). The organic layer was dried over Na_2SO_4 and evaporated. The residue was purified by FC (silica gel, column 10 x 2 cm, CH_2Cl_2/methanol, 10:1) giving **8** (154 mg, 0.19 mmol, 79% yield) as a light yellow foam. TLC (silica gel, CH_2Cl_2/acetone, 1:1): R_f 0.41. ^{31}P NMR (121 MHz, $CDCl_3$): δ 148.76, 149.18. ESI-TOF: *m/z* calcd. for $C_{44}H_{49}N_6O_8P$ $[M + H]^+$ 821.3422, found 821.3477.

Table S1. ^{13}C NMR chemical shifts of compounds **1**, **3**, **5** and **7**. [a]

	C(2)[b] C(2)[c]	C(4)[b] C(7a)[c]	C(5)[b] C(4a)[c]	C(6)[b] C(4)[c]	C(8)[b] C(6)[c]	C(1')	C(2')	C(3')	C(4')	C(5')	OMe	Furan
1	153.8	160.1	122.7	135.1	146.6	87.0	41.2	69.2	87.7	60.4	--	--
3	153.1	160.9	124.4	133.7	144.3	87.0	41.2	69.2	87.7	60.4	--	112.3, 112.6, 113.0, 145.8
5	152.5	159.3	124.4	135.4	147.4	87.3	40.9	70.0	86.1	63.3	54.8, 54.9	--
7	158.0[d]	161.2	126.7[d]	133.3	144.8	87.2	40.3	69.9	86.1	63.6	54.9	112.5, 113.2, 113.3, 146.1

[a] Measured in DMSO-d_6 at 298 K. [b] Purine numbering. [c] Systematic numbering. [d] Tentative.

Table S2. Selected ^{1}H-^{13}C coupling constants (Hz) of nucleosides **1**, **3**, **5** and **7**. [a]

	1	**3**	**5**	**7**
^{1}J(C6, H-C6)	185.5	185.2	184.3	183.0
^{1}J(C1', H-C1')	175.5	173.0	175.2	174.8
^{1}J(C3', H-C3')	147.9	147.4	150.2	150.6
^{1}J(C4', H-C4')	147.3	147.2	148.4	149.2
^{1}J(C5', H-C5')	141.6	139.5	140.2	141.0

[a] ^{1}H-^{13}C gated-decoupled NMR spectra were measured in DMSO-d_6 at 298 K.

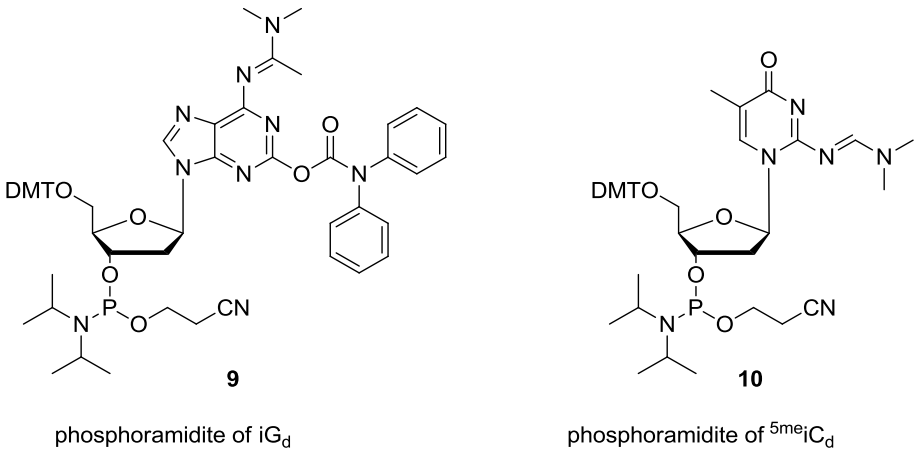

Fig. S1. Structures of phosphoramidites iG$_d$ (**9**) and ^{5me}iC$_d$ (**10**).

Quantum yield determination.

The fluorescence quantum yield (Φ_f) was determined by a relative method with quinine sulfate in 0.1 M H_2SO_4 ($\Phi_f = 0.54$) as a reference standard.[3] The quantum yield of the unknown $\Phi_{(x)}$ can be calculated by the following equation:

$$\Phi_{(x)} = \Phi_{(ST)}(A_{ST}/A_X)(F_X/F_{ST})(\eta^2_X/\eta^2_{ST})$$

Where $\Phi_{(ST)}$ is the quantum yield of the standard, A is the absorbance at the excitation wavelength, F is the integrated area in the emission curve, the subscripts X and ST refer to unknown and standard and η is the refractive index of solvent.

Table S3. Photophysical properties of fluorescent nucleosides.

Compounds	λ_{max} [nm]	ε_{max} [$mol^{-1}dm^3cm^{-1}$]	Ex_{max} [nm]	Em_{max} [nm]	Quantum yield (Φ) [a]
1	324	3700	324	388	0.03 [b]
2	344	13500	342	398	0.33 [b]
3	346	14800	350	399	0.39 [b]

[a] Quantum yields were determined using quinine sulfate in 0.1 M H_2SO_4 as standard with $\Phi = 0.54$.

[b] Determined in methanol.

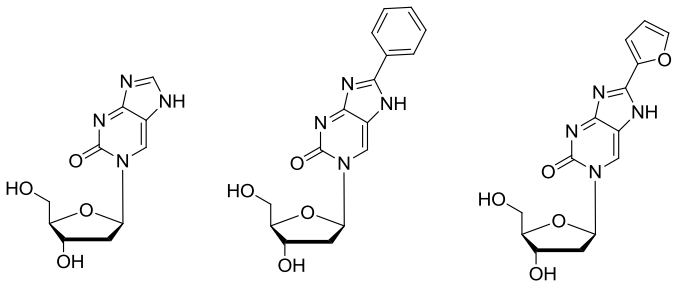

pK_a Determination by fluorescence and UV.

Nucleosides **1** or **3** were dissolved in 0.1 M sodium phosphate buffer, pH 4.5. NaOH solution (4 M) and concentrated phosphorus acid was used to adjust the pH value of the buffer. At defined pH values, the fluorescence of nucleoside **1** or **3** was measured. At each pH value emission spectra were measured with excitation at 324 nm for **1** and 350 nm for **3**. The fluorescence intensity at 388 nm for **1** and 400 nm for **3** were recorded to determine the pK_a values of nucleosides **1** and **2**. For comparison, the pK_a values of nucleosides **1** and **2** were also determined UV-spectrophotometrically.

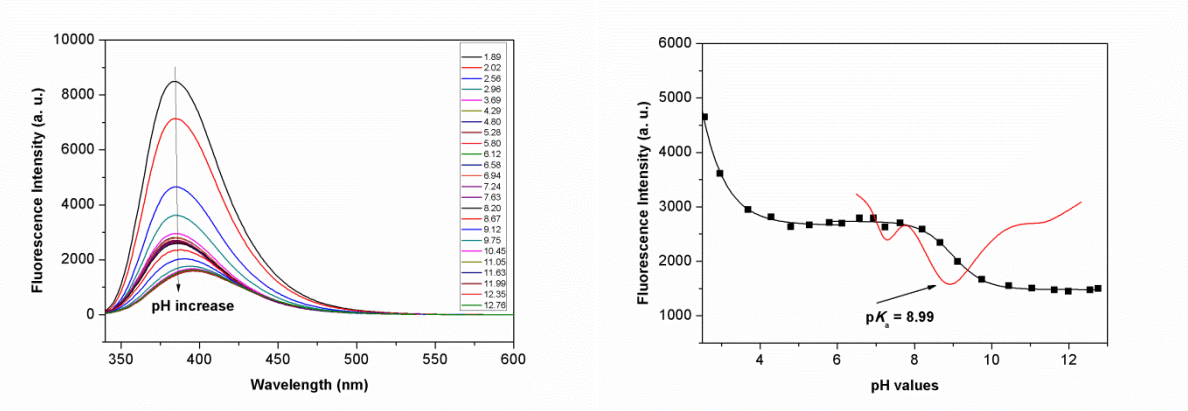

(a) (b)

Fig. S2 (a) pH Dependent fluorescence spectra of nucleoside **1**. The excitation wavelength was set to 324 nm. (b) Fluorescence intensity (a.u.) *vs* pH-value and its first derivative using data from (a).

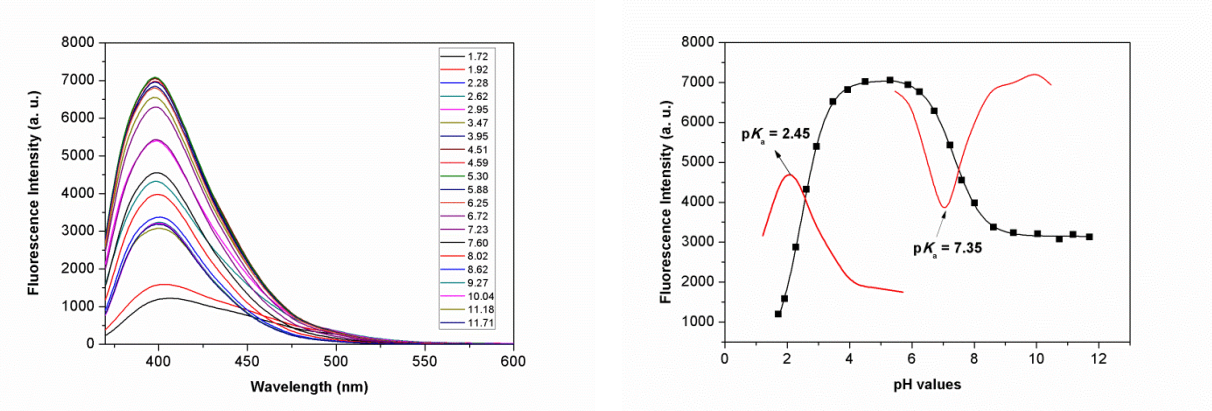

(a) (b)

Fig. S3 (a) pH Dependent fluorescence spectra of nucleoside **3**. The excitation wavelength was set to 350 nm. (b) Fluorescence intensity (a.u.) *vs* pH-value and its first derivative using data from (a).

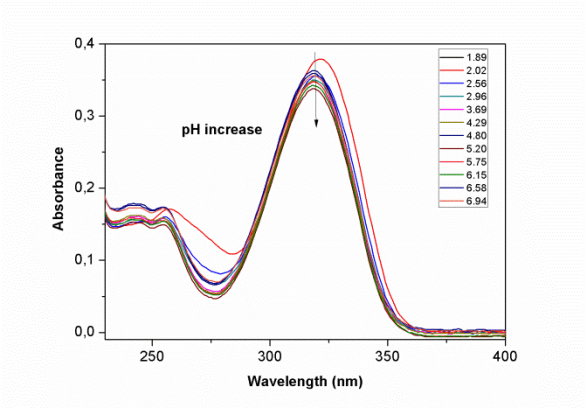

(a)

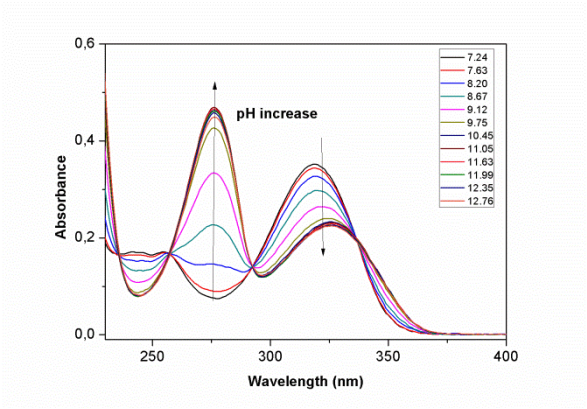

(b)

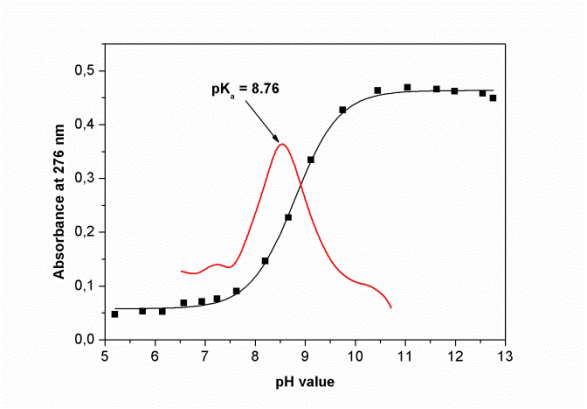

(c)

Fig. S4 (a) and (b) UV spectroscopic change of nucleoside **1** at various pH values and (c) absorbance at 276 nm *vs* pH-value and its first derivative using data from (b).

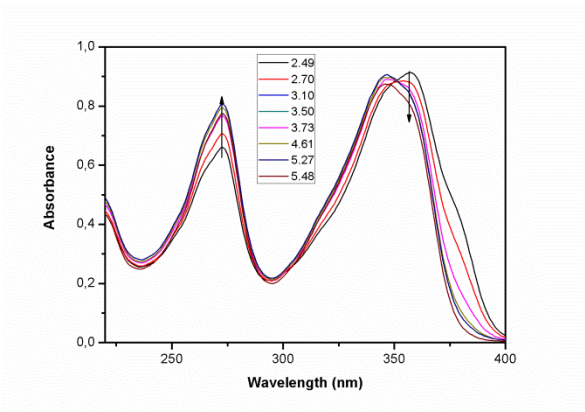

(a)

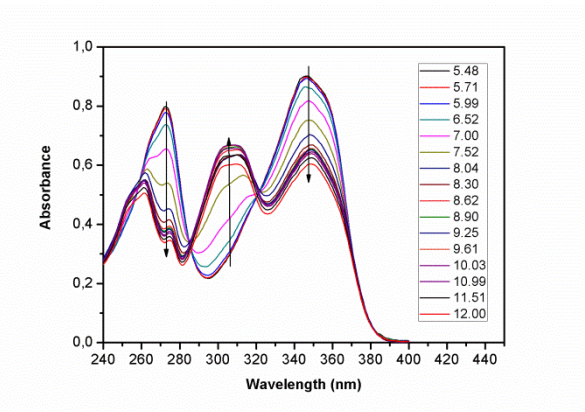

(b)

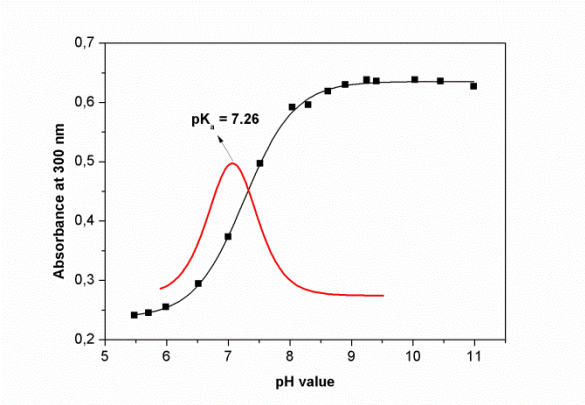

(c)

Fig. S5 (a) and (b) UV spectroscopic change of nucleoside **3** at various pH values and (c) absorbance at 300 nm *vs* pH-value and its first derivative using data from (b).

Table S4. Molecular masses of oligonucleotides measured by MALDI-TOF mass spectrometry.[a]

Oligonucleotides	Molecular Weight [u]	
	$[M+H]^+$ Calc.	**$[M+H]^+$ Found**
5'-d(TAG GT**1** AAT ACT) ODN-**3**	3670.4	3671.3
5'-d(ATiC iCA **1** TTA TiGA) ODN-**4**	3658.5	3655.6
5'-d(ATiC iCA **2** TTA TiGA) ODN-**6**	3734.5	3731.4
5'-d(TAG GT**3** AAT ACT) ODN-**7**	3736.5	3734.9
5'-d(ATiC iCA **3** TTA TiGA) ODN-**8**	3724.5	3722.7
5'-d(AGT ATT **1**AC CTA) ODN-**10**	3630.5	3629.0
5'-d(AGT ATT **3**AC CTA) ODN-**12**	3696.5	3695.4
5'-d(TiCA TAA **1**TiG iGAT) ODN-**14**	3684.5	3683.0
5'-d(TiCA TAA **2**TiG iGAT) ODN-**15**	3760.5	3762.3
5'-d(TiCA TAA **3**TiG iGAT) ODN-**16**	3750.5	3750.8

[a] Measured in the linear positive mode. iC corresponds to $^{5me}iC_d$.

HPLC profiles of oligonucleotides determined at 260 nm.

HPLC (RP-18) profiles of single-stranded oligonucleotides determined at 260 nm. For elution the following solvent system was used: 0.1 M (Et_3NH)OAc (pH 7.0) : MeCN (95:5) (A) and MeCN (B). Gradient: 0-20 min 0-20% B in A, 20-25 min 20% B in A, 25-30 min 20-0% B in A, flow rate 0.8 mL min^{-1}.

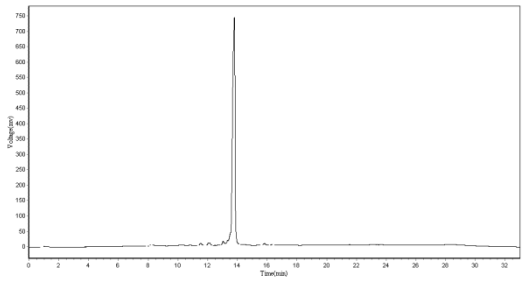

(a)

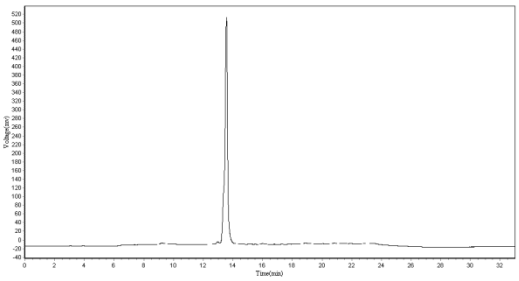

(b)

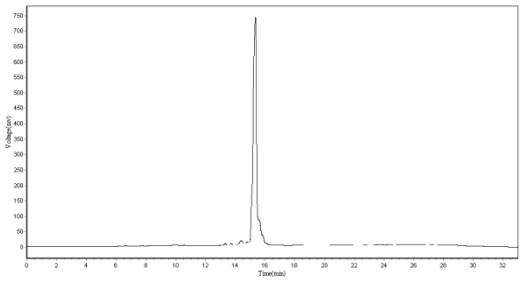

(c)

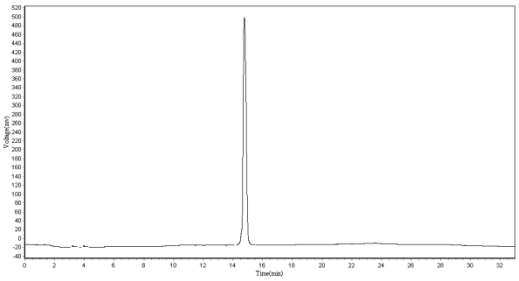

(d)

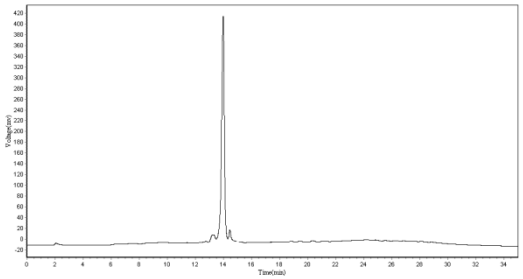

(e)

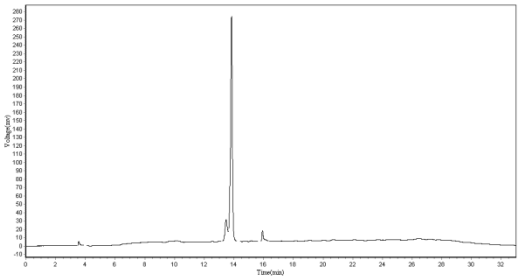

(f)

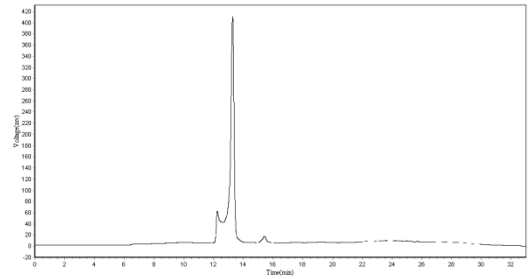

(g)

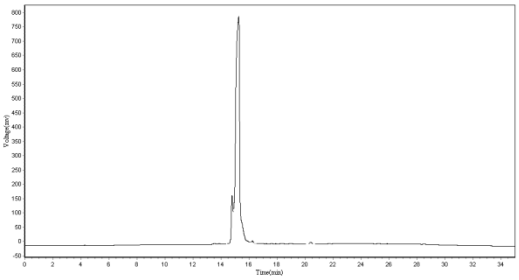

(h)

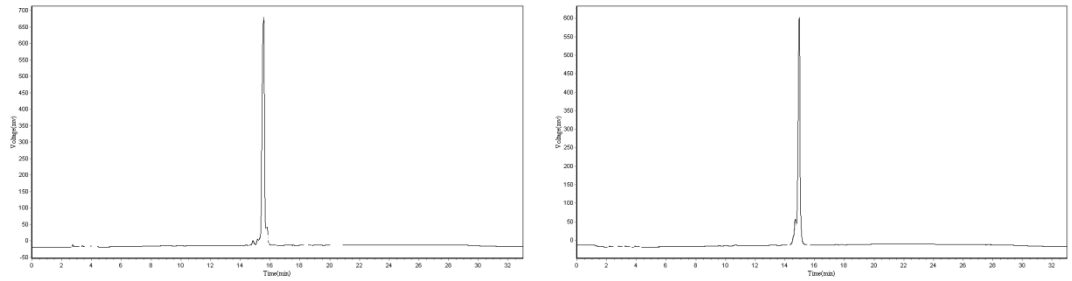

(i) (j)

Fig. S6 HPLC profiles of oligonucleotides. (a) 5'-d(TAG GT**1** AAT ACT) ODN-**3**, (b) 5'-d(ATiCiCA**1**TTATiGA) ODN-**4**, (c) 5'-d(ATiCiCA**2**TTATiGA) ODN-**6**, (d) 5'-d(TAG GT**3** AAT ACT) ODN-**7**, (e) 5'-d(ATiCiCA**3**TTATiGA) ODN-**8**, (f) 3'-d(ATC CA**1** TTA TGA) ODN-**10**, (g) 5'-d(TiCATAA**1**TiGiGAT) ODN-**14**, (h) 5'-d(TiCATAA**2**TiGiGAT) ODN-**15**, (i) 3'-d(ATC CA**3** TTA TGA) ODN-**12**, (j) 5'-d(TiCATAA**3**TiGiGAT) ODN-**16**. X-axis refers to time (min), Y-axis refers to UV-absorbance at 260 nm (a.u.).

Stoichiometric titration.

To a solution containing 5 μM + 5 μM of the single-stranded oligonucleotides in 1 mL of 100 mM NaOAc, 10 mM $Mg(OAc)_2$ buffer (pH 7.5) was added 2 μL of a 1 mM $AgNO_3$ stock solution in bid. H_2O. Thus, a ratio of the silver/duplex of 0.4:1 was obtained. Then, in a stepwise manner 2 μL of the $AgNO_3$ stock solution were added until a final ratio of silver to DNA duplex of 4:1 was reached. After each addition of the stock solution, the mixture was equilibrated for 5 min (at 20 °C). The UV-absorption spectra were recorded in the range of 220-450 nm and fluorescence emission spectra were recorded in the range of 380-600 nm. Titration studies on ps duplexes ODN-**3** • ODN-**4**, ODN-**5** • ODN-**6**, ODN-**7** • ODN-**8**, ODN-**10** • ODN-**14**, ODN-**11** • ODN-1**5**, ODN-**12** • ODN-**16** and aps duplexes ODN-**3** • ODN-**10**, and ODN-**7** • ODN-**12** were performed according to this procedure. Then, the UV absorbance changes at selected wavelengths were plotted vs the ratio of silver/duplex to establish the stoichiometry.

Titration studies on monomeric nucleosides **1** and **3** (10 μM) were also performed using the procedure described above.

Stoichiometric titration of nucleosides.

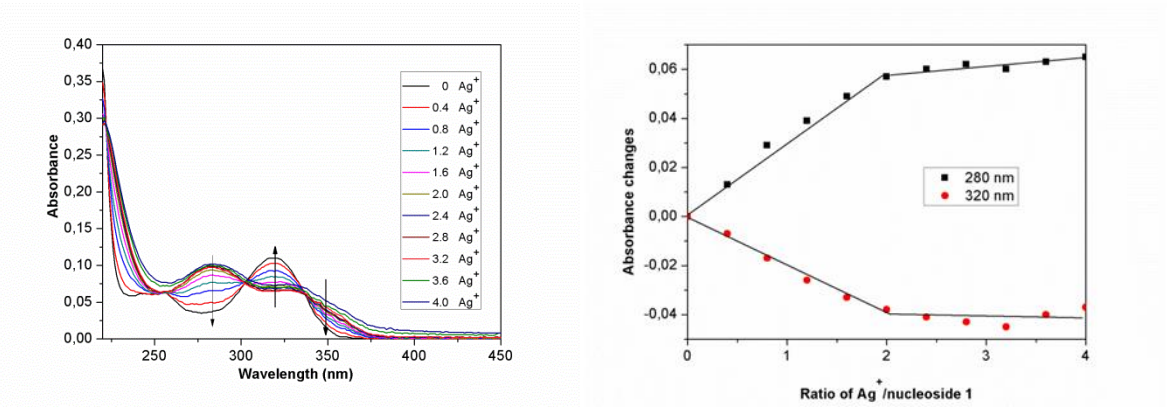

(a) (b)

Fig. S7 (a) UV spectrophotometric titration of nucleoside **1** (10 μM) with increasing concentration of Ag^+ ions (0–4.0 equiv) in buffer solution (100 mM NaOAc, 10 mM $Mg(OAc)_2$, pH = 7.5) containing 0.5% DMSO at 20 °C. (b) Graph of ratio of equivalents of silver ions/nucleoside **1** versus changes in absorbance at different wavelengths from (a).

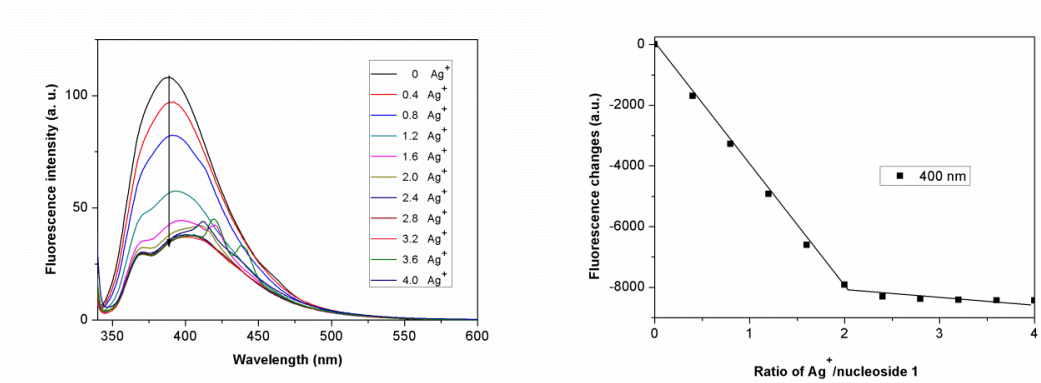

(a) (b)

Fig. S8 (a) Fluorescence spectra of nucleoside **1** with increasing concentration of Ag^+ ions (0–4.0 equiv) in buffer solution (100 mM NaOAc, 10 mM $Mg(OAc)_2$, pH = 7.5) containing 0.5% DMSO at 20 °C. b) Graph of ratio of equivalents of silver ions/nucleoside **1** versus changes in fluorescence intensity (a. u.) at 400 nm. The excitation wavelength was set to 324 nm.

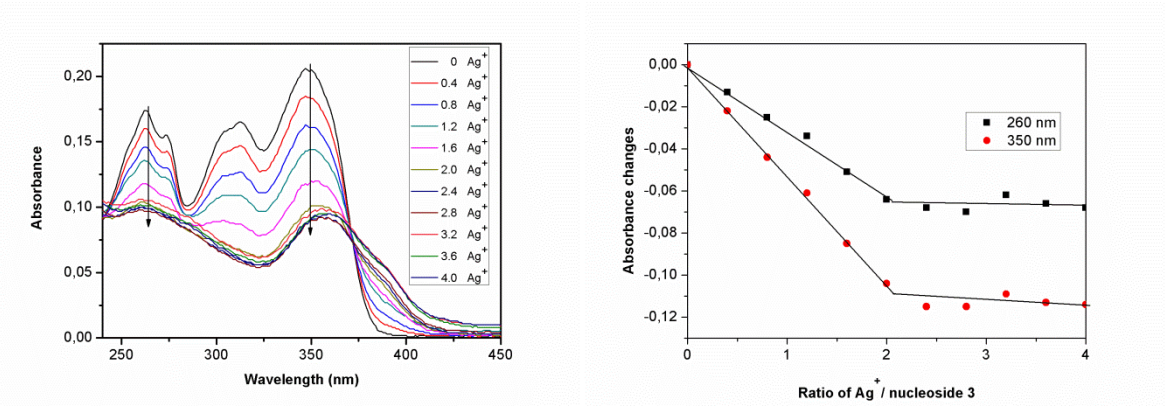

(a) (b)

Fig. S9 (a) UV spectrophotometric titration of nucleoside **3** (10 μM) with increasing concentration of Ag^+ ions (0-4.0 equiv) in buffer solution (100 mM NaOAc, 10 mM $Mg(OAc)_2$, pH = 7.5) containing 0.5% DMSO at 20 °C. (b) Graph of ratio of equivalents of silver ions/nucleoside **3** versus changes in absorbance at different wavelengths from (a).

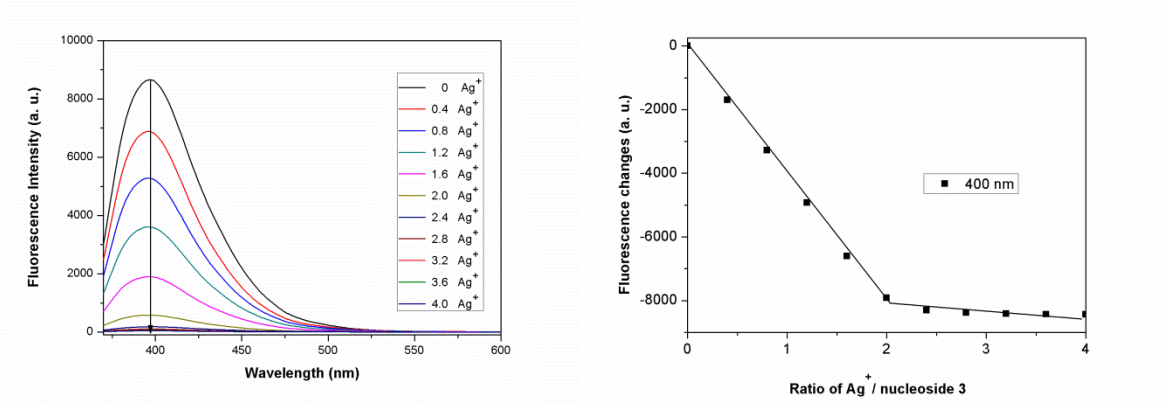

(a) (b)

Fig. S10 (a) Fluorescence spectra of nucleoside **3** with increasing concentration of Ag^+ ions (0-4.0 equiv) in buffer solution (100 mM NaOAc, 10 mM $Mg(OAc)_2$, pH = 7.5) containing 0.5% DMSO at 20 °C. b) Graph of ratio of equivalents of silver ions/nucleoside **3** versus changes in fluorescence intensity (a. u.) at 400 nm. The excitation wavelength was set to 350 nm.

Stoichiometric titration of oligonucleotides.

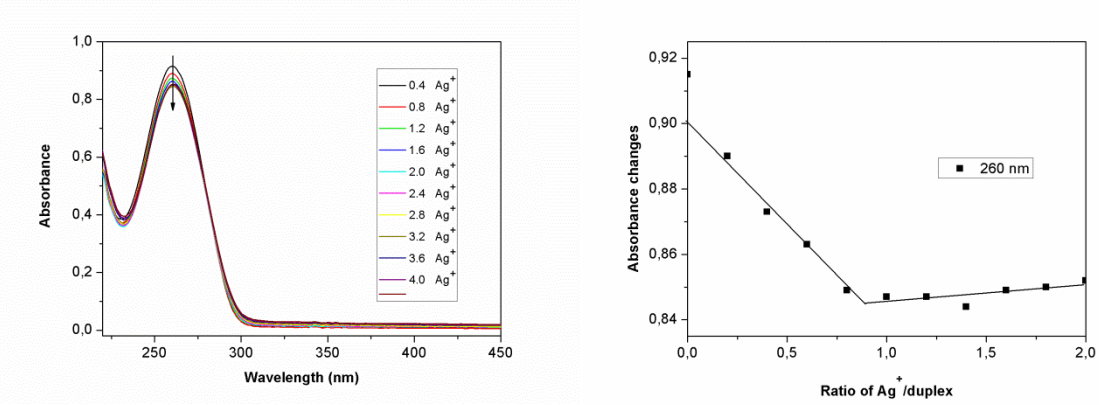

(a) (b)

Fig. S11 (a) UV titration of ODN-**1** • ODN-**1a** (5 µM + 5 µM) with increasing Ag^+ concentration in 100 mM NaOAc, 10 mM $Mg(OAc)_2$, pH = 7.5. (b) Graph of ratio of equivalents of silver ions/duplex versus changes in absorbance at 260 nm.

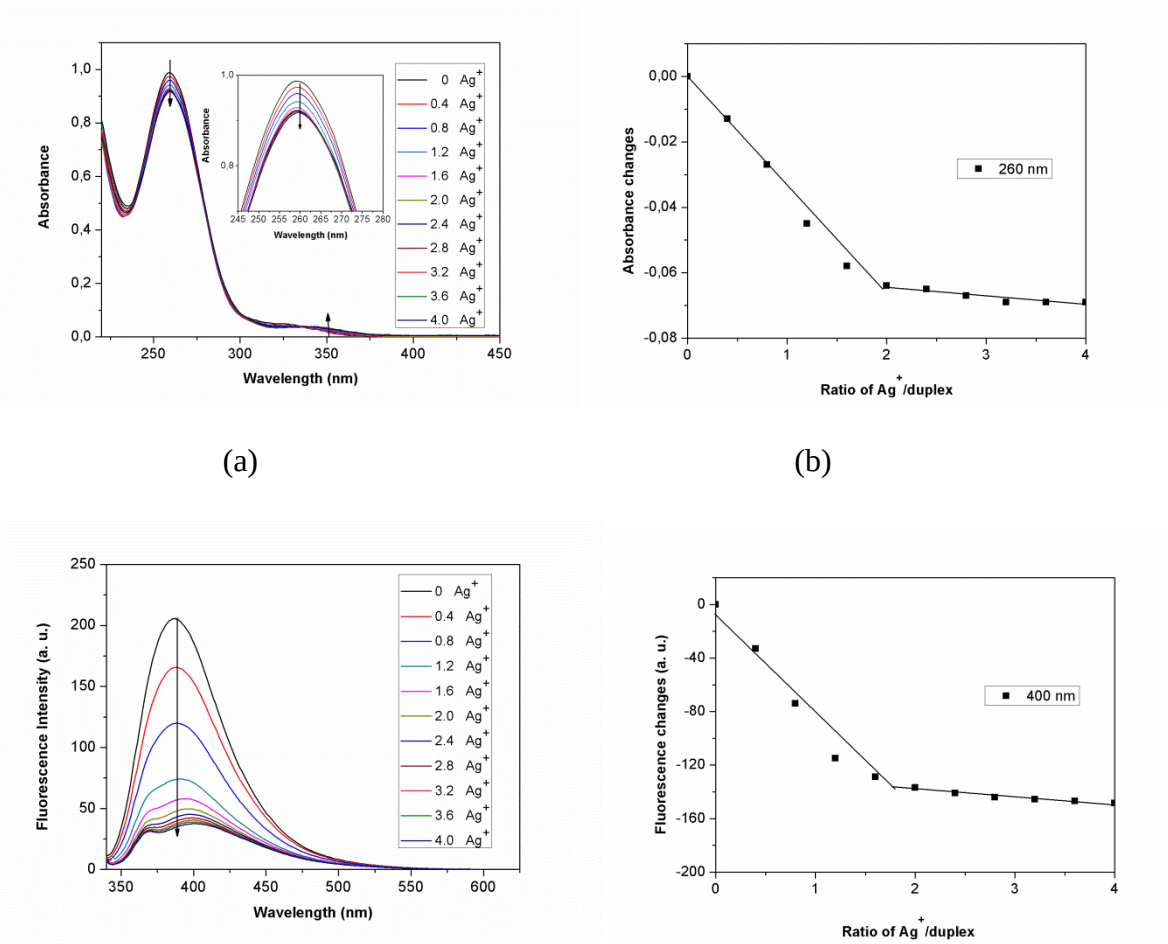

Fig. S12 (a) UV and (c) fluorescence titration of ODN-**3** • ODN-**4** (5 μM + 5 μM) with increasing Ag^+ concentration in 100 mM NaOAc, 10 mM $Mg(OAc)_2$, pH = 7.5. (b) and (d) Determination of the silver to duplex ratio at different wavelengths from (a) and (c).

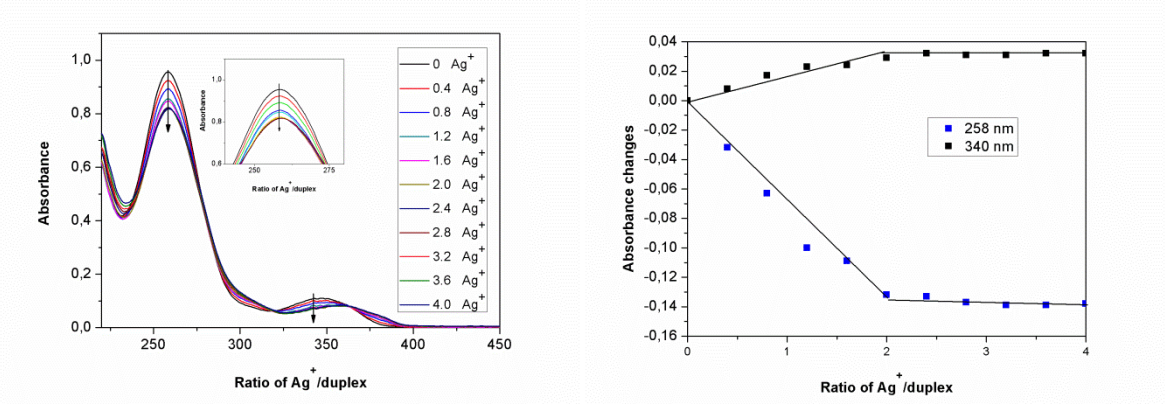

(a) (b)

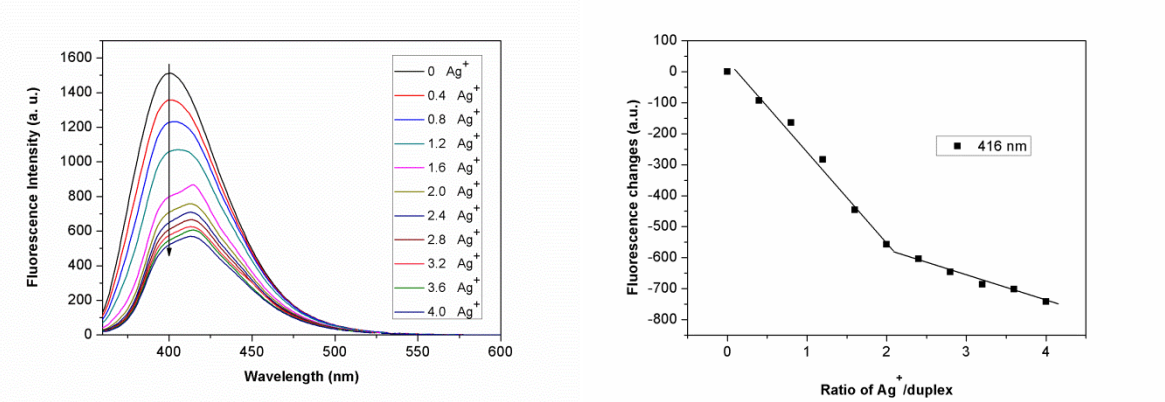

(c) (d)

Fig. S13 (a) UV and (c) fluorescence titration of ODN-**5** • ODN-**6** (5 µM + 5 µM) with increasing Ag^+ concentration in 100 mM NaOAc, 10 mM $Mg(OAc)_2$, pH = 7.5. (b) and (d) Determination of the silver to duplex ratio at different wavelengths from (a) and (c).

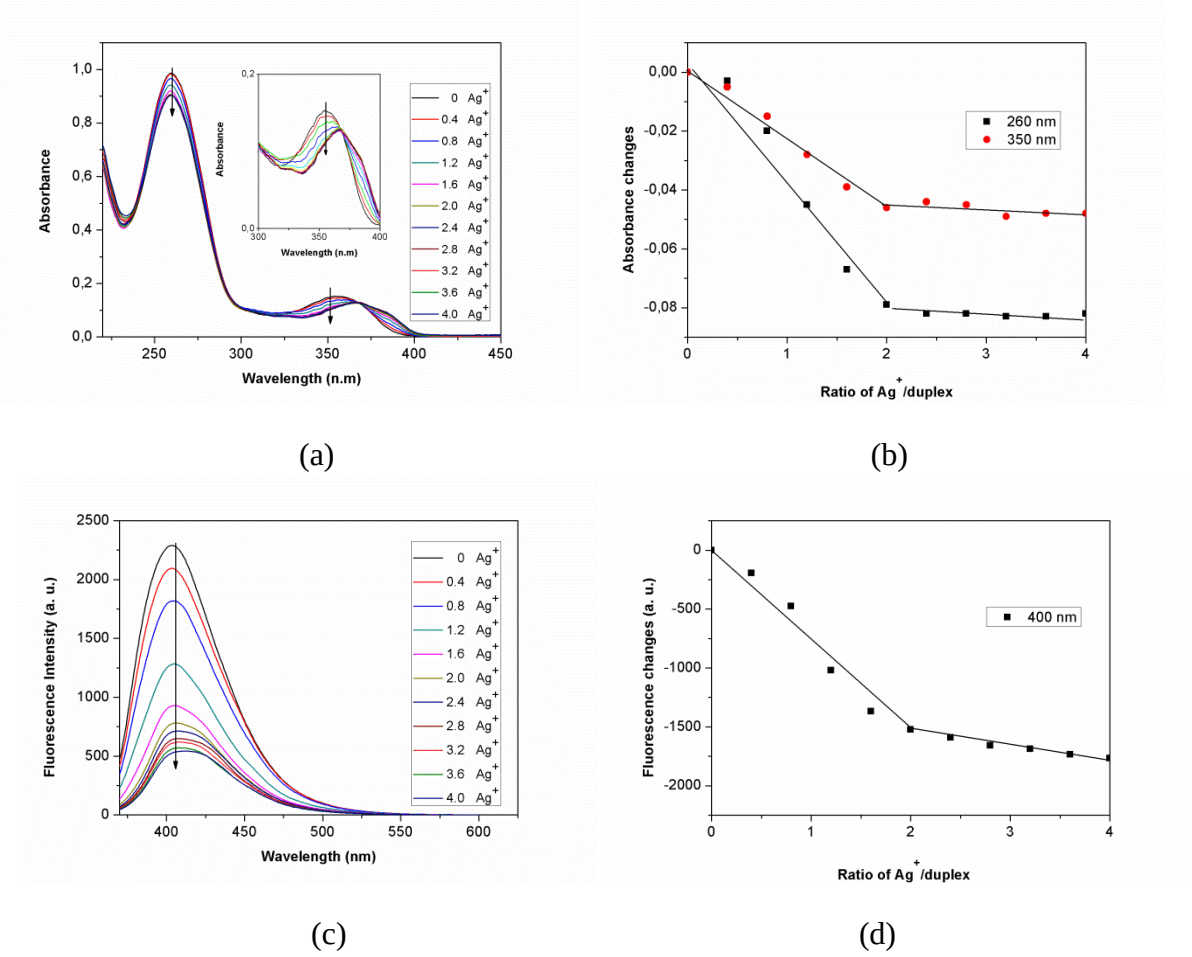

Fig. S14 (a) UV and (c) fluorescence titration of ODN-**7** • ODN-**8** (5 µM + 5 µM) with increasing Ag^+ concentration in 100 mM NaOAc, 10 mM $Mg(OAc)_2$, pH = 7.5. (b) and (d) Determination of the silver to duplex ratio at different wavelengths from (a) and (c).

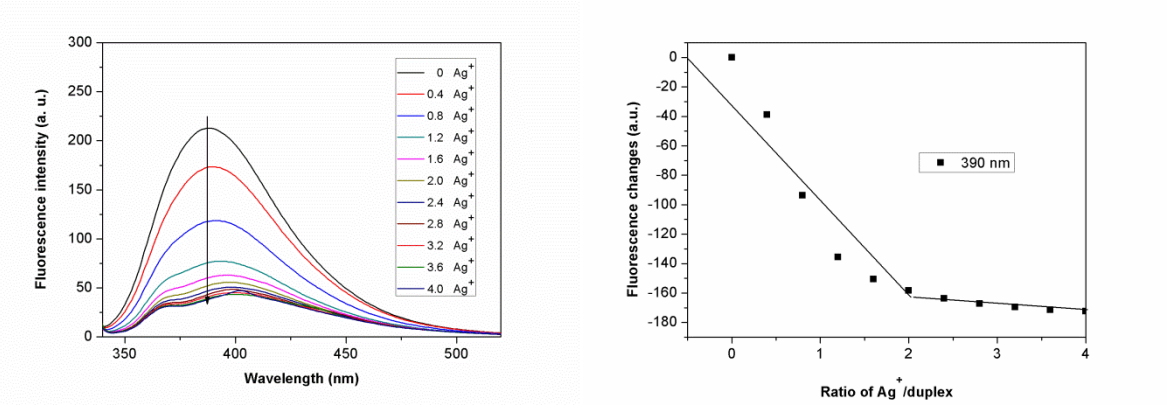

(a) (b)

Fig. S15 (a) Fluorescence titration of ODN-**10** • ODN-**14** (5 μM + 5 μM) with increasing Ag^+ concentration in 100 mM NaOAc, 10 mM $Mg(OAc)_2$, pH = 7.5. (b) Determination of the silver to duplex ratio at different wavelengths from (a).

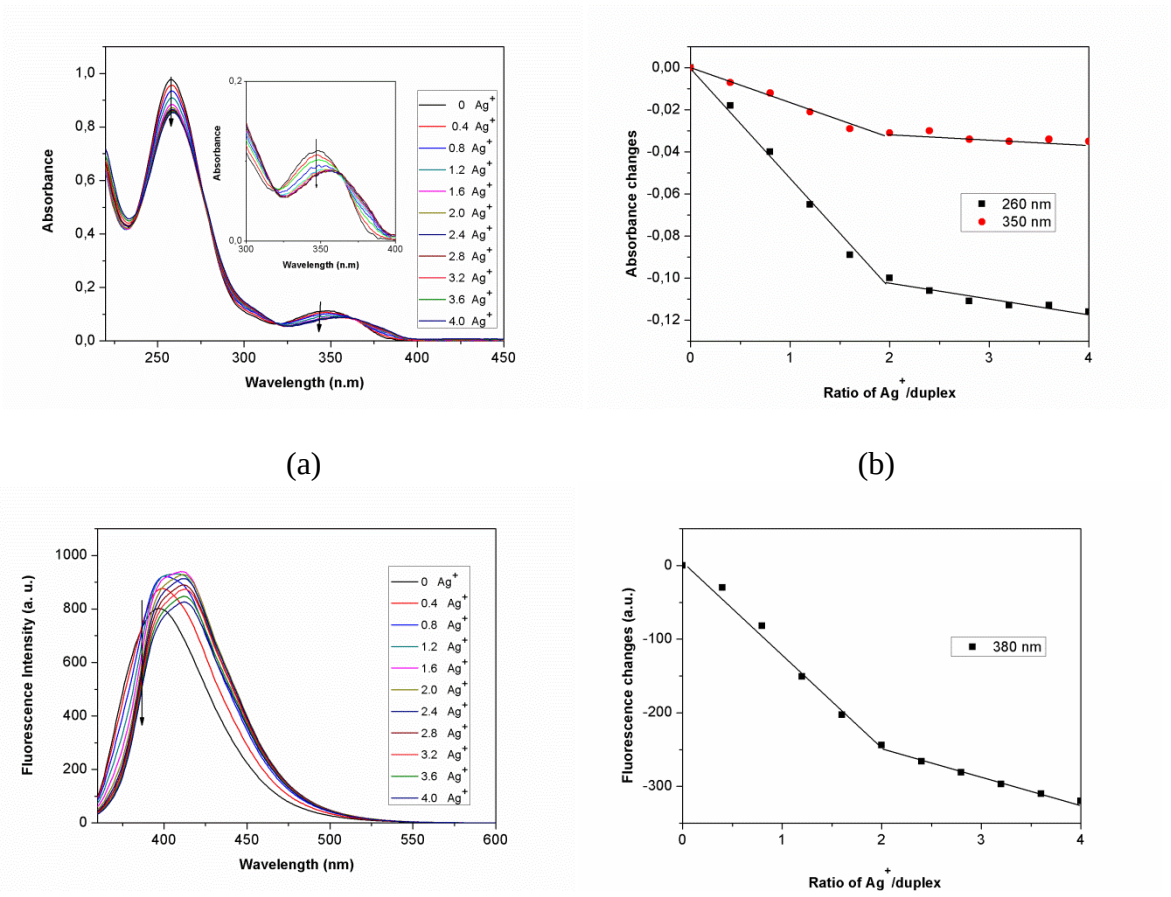

Fig. S16 (a) UV and (c) fluorescence titration of ODN-**11** • ODN-**15** (5 μM + 5 μM) with increasing Ag^+ concentration in 100 mM NaOAc, 10 mM $Mg(OAc)_2$, pH = 7.5. (b) and (d) Determination of the silver to duplex ratio at different wavelengths from (a) and (c).

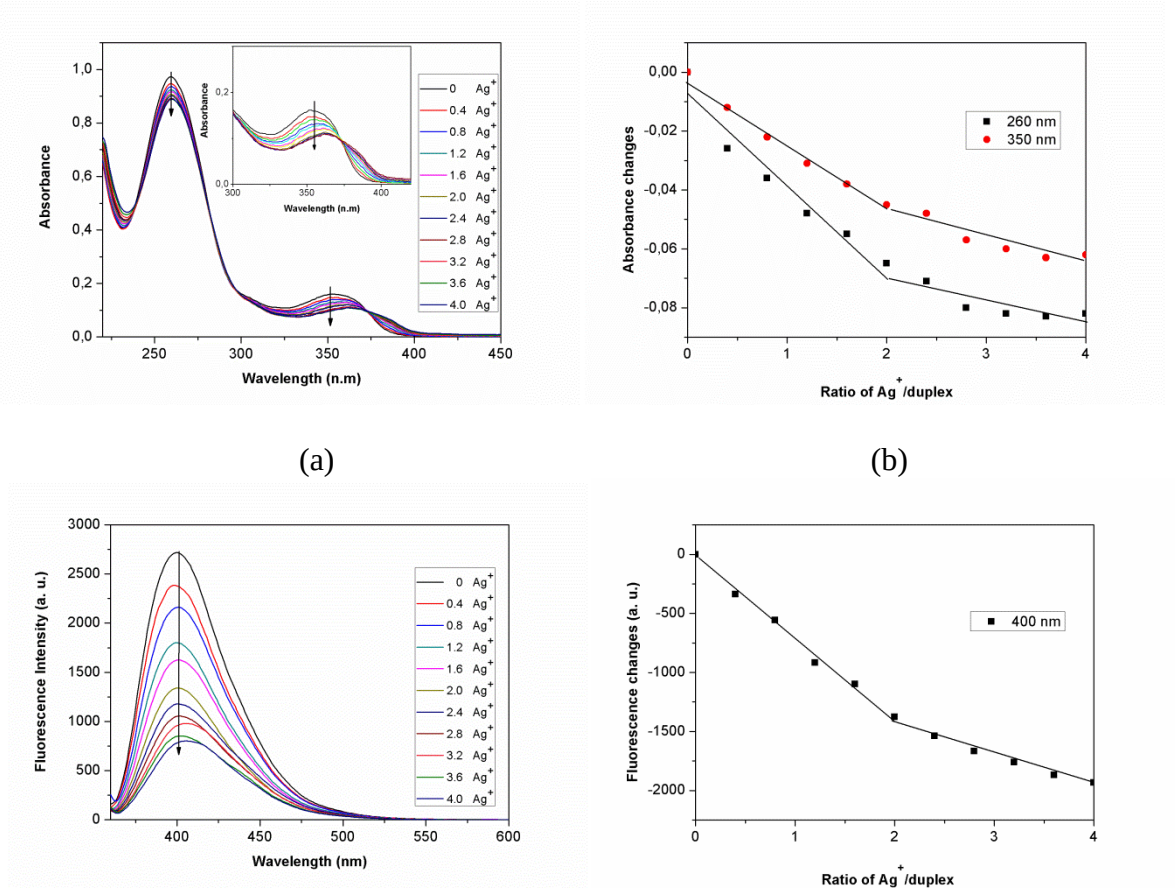

(a) (b)

(c) (d)

Fig. S17 (a) UV and (c) fluorescence titration of ODN-**12** • ODN-**16** (5 μM + 5 μM) with increasing Ag^+ concentration in 100 mM NaOAc, 10 mM $Mg(OAc)_2$, pH = 7.5. (b) and (d) Determination of the silver to duplex ratio at different wavelengths from (a) and (c).

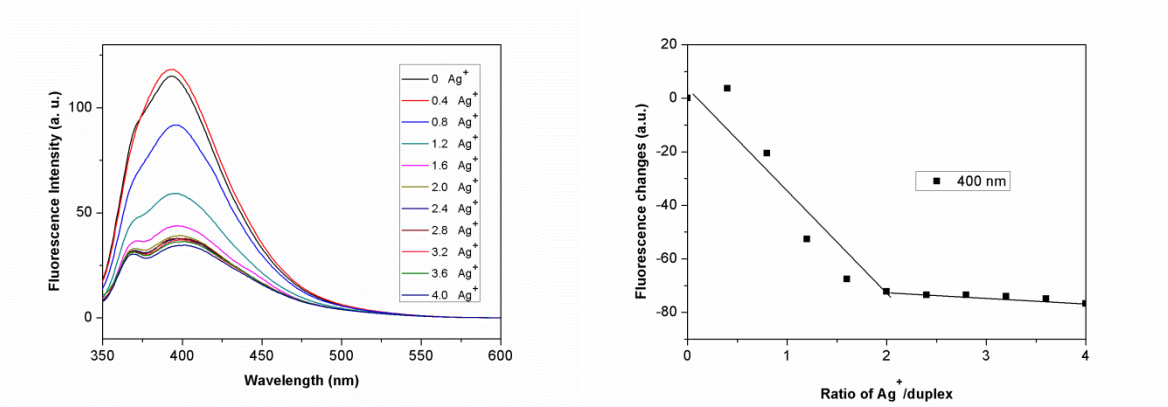

(a) (b)

Fig. S18 (a) Fluorescence titration of ODN-**3** • ODN-**10** (5 μM + 5 μM) with increasing Ag^+ concentration in 100 mM NaOAc, 10 mM $Mg(OAc)_2$, pH = 7.5. (b) Determination of the silver to duplex ratio at different wavelengths from (a).

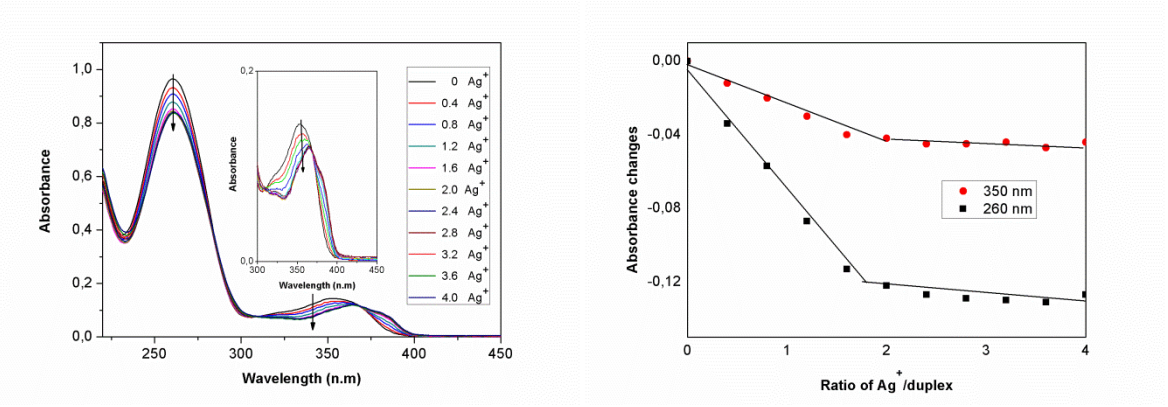

(a) (b)

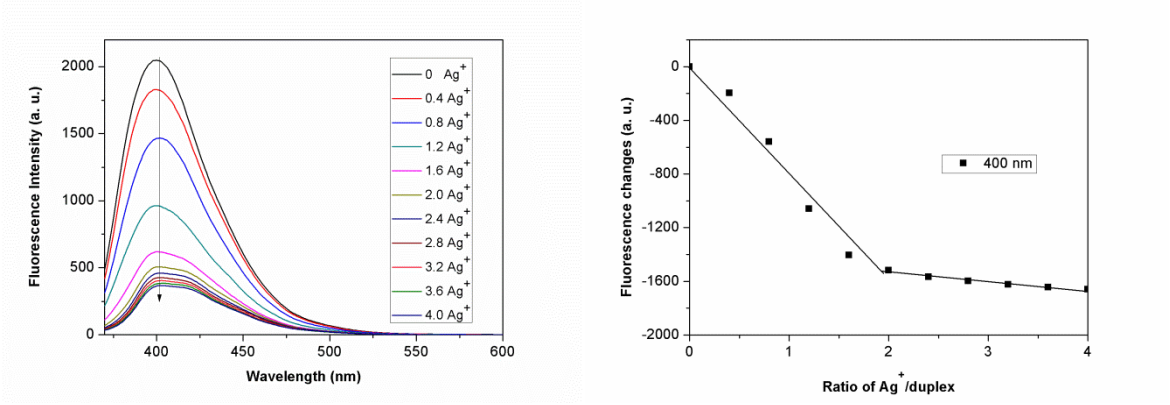

(c) (d)

Fig. S19 (a) UV and (c) fluorescence titration of ODN-**7** • ODN-**12** (5 μM + 5 μM) with increasing Ag^+ concentration in 100 mM NaOAc, 10 mM $Mg(OAc)_2$, pH = 7.5. (b) and (d) Determination of the silver to duplex ratio at different wavelengths from (a) and (c).

Table S5. T_m values of DNA duplexes containing ImidC derivatives (**1**-**3**) in the presence or absence of silver ions.[a]

Duplexes	T_m [°C] with n equiv of $AgNO_3$			ΔT_m [°C] relative to mismatch[b]
	$n = 0$	$n = 1$	$n = 2$	
ps duplex DNA (pattern 1)				
5'-d(TAG GT**1** AAT ACT) ODN-**3** 5'-d(ATiC iCA**1** TTA TiGA) ODN-**4**	n.d.	n.d./53.0[c]	53.0	n.d.
5'-d(TAG GT**2** AAT ACT) ODN-**5** 5'-d(ATiC iCA**2** TTATiGA) ODN-**6**	27.0	n.d./54.0[c]	54.0	+27.0
5'-d(TAG GT**3** AAT ACT) ODN-**7** 5'-d(ATiC iCA**3** TTA TiGA) ODN-**8**	25.0	20.0/63.0[c]	63.0	+38.0
ps duplex DNA (pattern 2)				
5'-d(AGT ATT **1**AC CTA) ODN-**10** 5'-d(TiCA TAA **1**TiG iGAT) ODN-**14**	n.d.	n.d./53.0[c]	53.0	n.d.
5'-d(AGT ATT **2**AC CTA) ODN-**11** 5'-d(TiCA TAA **2**TiG iGAT) ODN-**15**	n.d.	n.d./53.0[c]	53.0	n.d.
5'-d(AGT ATT **3**AC CTA) ODN-**12** 5'-d(TiCA TAA **3**TiG iGAT) ODN-**16**	n.d.	n.d./59.0[c]	59.0	n.d.
aps duplex DNA				
5'-d(TAG GT**C** AAT ACT) ODN-**1** 3'-d(ATC CA**G** TTA TGA) ODN-**9**	42.5	43.0	41.5	-1.0
5'-d(TAG GT**1** AAT ACT) ODN-**3** 3'-d(ATC CA**1** TTA TGA) ODN-**10**	23.0	27.0/66.0[c]	65.0	+42.0
5'-d(TAG GT**2** AAT ACT) ODN-**5** 3'-d(ATC CA**2** TTA TGA) ODN-**11**	32.5	31.5/70.0[c]	71.0	+38.5
5'-d(TAG GT**3** AAT ACT) ODN-**7** 3'-d(ATC CA**3** TTA TGA) ODN-**12**	26.0	26.0/74.0[c]	74.5	+48.5

[a] Measured at 260 nm with 5 µM + 5 µM single-strand concentration at a heating rate of 1.0 °C/min in 100 mM NaOAc pH 7.3 in the presence of various concentrations of $AgNO_3$ (0-2.0 equivalents). Melting was performed in the range of 15-90°C. T_m values were calculated from the heating curves. [b] $\Delta T_m = T_m$ after the addition of 2.0 equivalents $AgNO_3 - T_m$ before the addition of $AgNO_3$. [c] Biphasic melting. n.d. not determined.

Table S6. T_m values and thermodynamic data of duplexes with parallel and antiparallel chain orientation[a,b]

Duplexes		eq. of Ag^+	T_m [°C]	-ΔH [c] [kcal/mol]	-ΔS [c] [cal/K/mol]	-ΔG [c] [kcal/mol]
ps duplex DNA (pattern I)						
5'-d(TAG GT**C** AAT ACT)	ODN-**1**	0	34.5	60.5	170.9	7.5
5'-d(ATiCiCA**iG** TTATiGA)	ODN-**2**	2	33.5	60.2	169.5	7.3
5'-d(TAG GT**1** AAT ACT)	ODN-**3**	0	28.0	57.4	165.0	6.2
5'-d(ATiCiCA**1** TTATiGA)	ODN-**4**	2	55.0	48.5	122.6	10.5
5'-d(TAG GT**2** AAT ACT)	ODN-**5**	0	31.0	64.6	186.9	6.6
5'-d(ATiCiCA**2** TTATiGA)	ODN-**6**	2	58.0	64.1	167.7	12.1
5'-d(TAG GT**3** AAT ACT)	ODN-**7**	0	29.0	58.5	167.8	6.5
5'-d(ATiCiCA**3** TTATiGA)	ODN-**8**	2	67.0	53.8	132.5	12.7
ps duplex DNA (pattern II)						
5'-d(AGT ATT **G**AC CTA)	ODN-**9**	0	42.0	88.9	256.2	9.4
5'-d(TiCA TAA **iC**TiG iGAT)	ODN-**13**	2	42.0	88.9	256.7	9.3
5'-d(AGT ATT **1**AC CTA)	ODN-**10**	0	28.0	63.0	183.6	6.1
5'-d(TiCA TAA **1**TiG iGAT)	ODN-**14**	2	57.0	62.9	164.6	11.8
5'-d(AGT ATT **2**AC CTA)	ODN-**11**	0	32.0	67.1	194.5	6.7
5'-d(TiCA TAA **2**TiG iGAT)	ODN-**15**	2	61.0	64.5	167.2	12.6
5'-d(AGT ATT **3**AC CTA)	ODN-**12**	0	28.0	62.4	181.3	6.2
5'-d(TiCA TAA **3**TiG iGAT)	ODN-**16**	2	66.0	58.6	147.4	12.9
aps duplex DNA						
5'-d(TAGGT**C**AATACT)	ODN-**1**	0	46.5	67.5	185.4	10.0
3'-d(ATCCA**G**TTATGA)	ODN-**9**	2	46.5	67.5	185.4	10.0
5'-d(TAGGT**1**AATACT)	ODN-**3**	0	32.0	50.9	141.3	7.1
3'-d(ATCCA**1**TTATGA)	ODN-**10**	2	71.0	- [d]	- [d]	- [d]
5'-d(TAGGT**3**AATACT)	ODN-**7**	0	30.0	62.5	180.1	6.6
3'-d(ATCCA**3**TTATGA)	ODN-**12**	2	78.0	- [d]	- [d]	- [d]

[a] Measured at 260 nm with 5 µM + 5 µM single-strand concentration at a heating rate of 1.0 °C/min in 100 mM NaOAc, 10 mM $Mg(OAc)_2$ pH 7.5 in the presence of various concentrations of $AgNO_3$ (0-2.0 equivalents). [b] See references 4a,b. [c] T_m values and thermodynamic data were determined with the program MeltWin 3.0 and are with 10% deviation. [d] T_m values are too high to get reliable thermodynamic data.

Melting profiles of oligonucleotides.

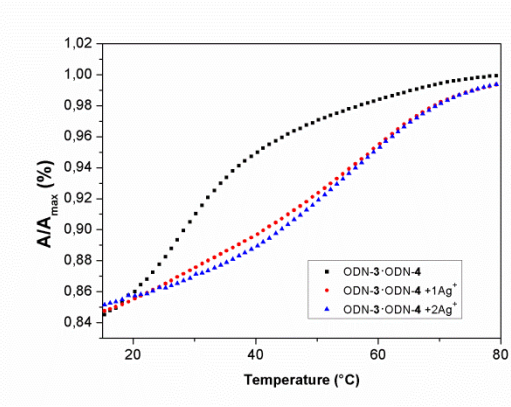

(a)

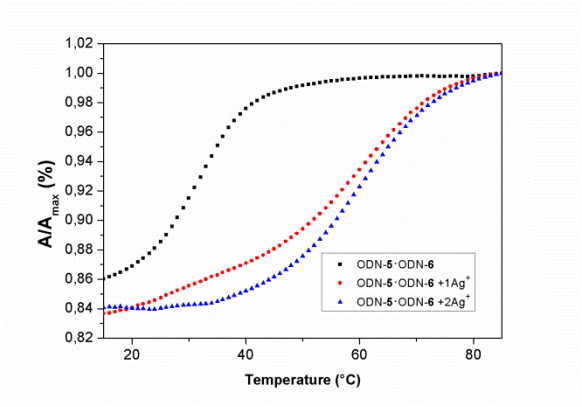

(b)

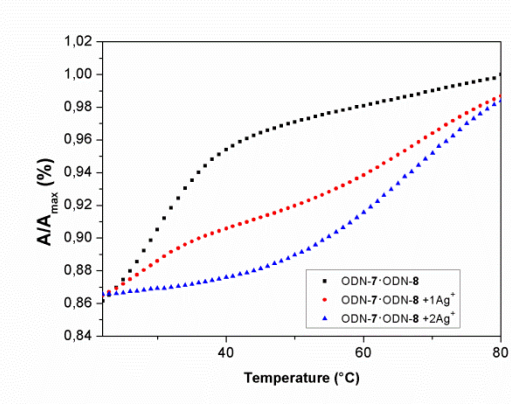

(c)

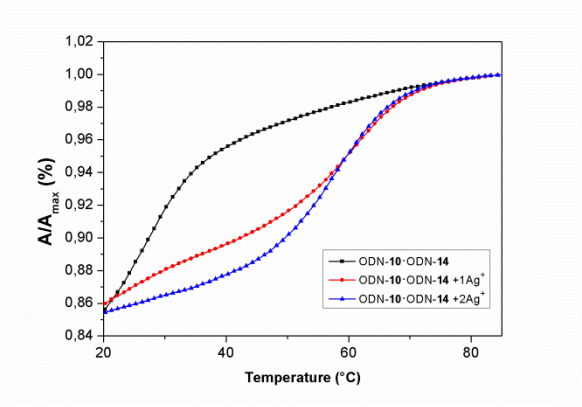

(d)

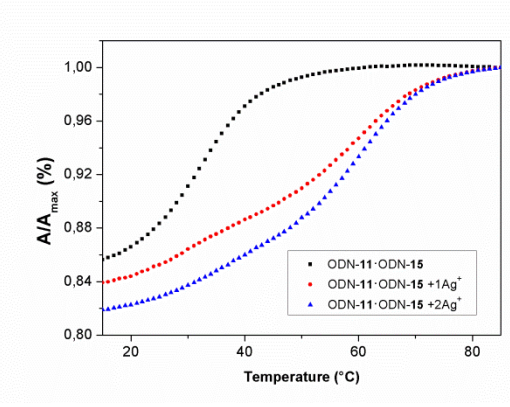

(e)

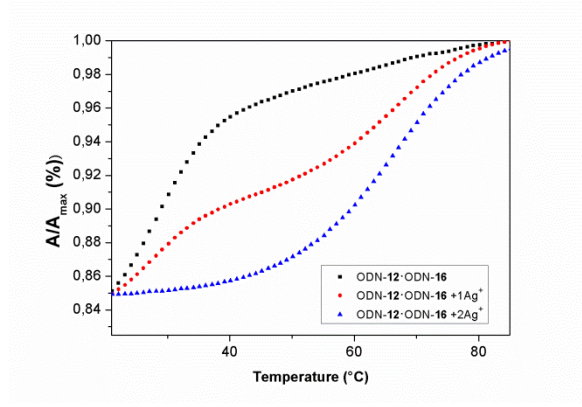

(f)

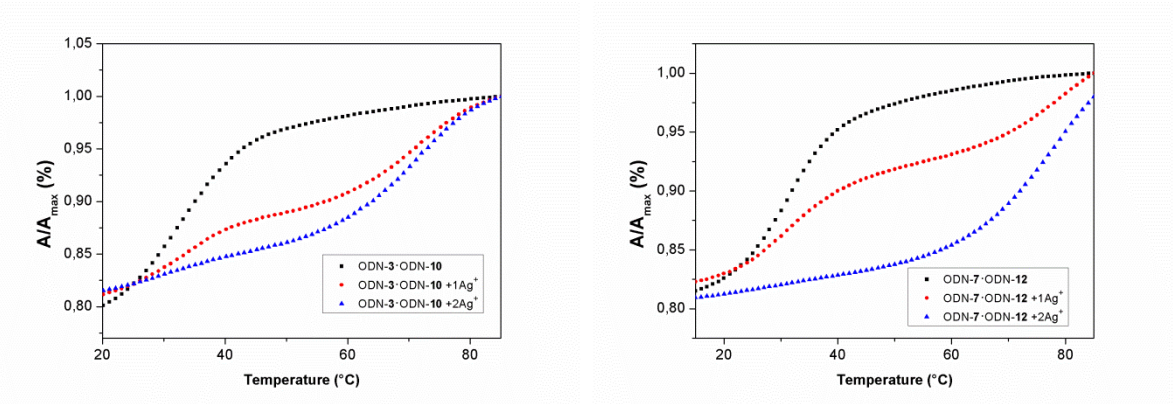

(g) (h)

Fig. S20 Thermal denaturation curves of ps and aps duplexes with increasing concentration of Ag^+ ions. The experiments were performed with 5 µM duplex concentration in 100 mM NaOAc, 10 mM $Mg(OAc)_2$ buffer (pH 7.5) at 260 nm. (a) ODN-**3** • ODN-**4**. (b) ODN-**5** • ODN-**6**. (c) ODN-**7** • ODN-**8**. (d) ODN-**10** • ODN-**14**. (e) ODN-**11** • ODN-**15**. (f) ODN-**12** • ODN-**16**. (g) ODN-**3** • ODN-**10**. (h) ODN-**7** • ODN-**12**.

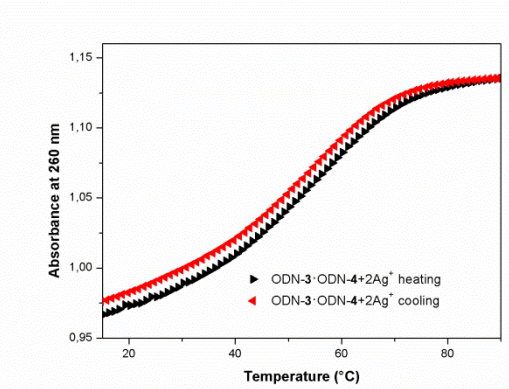
Absorbance at 260 nm
Temperature (°C)
ODN-3·ODN-4+2Ag+ heating
ODN-3·ODN-4+2Ag+ cooling

(a)

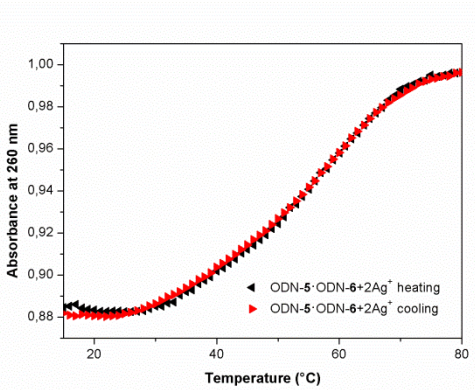
Absorbance at 260 nm
Temperature (°C)
ODN-5·ODN-6+2Ag+ heating
ODN-5·ODN-6+2Ag+ cooling

(b)

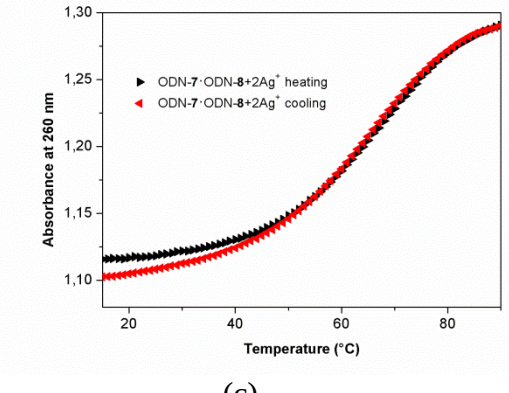
Absorbance at 260 nm
Temperature (°C)
ODN-7·ODN-8+2Ag+ heating
ODN-7·ODN-8+2Ag+ cooling

(c)

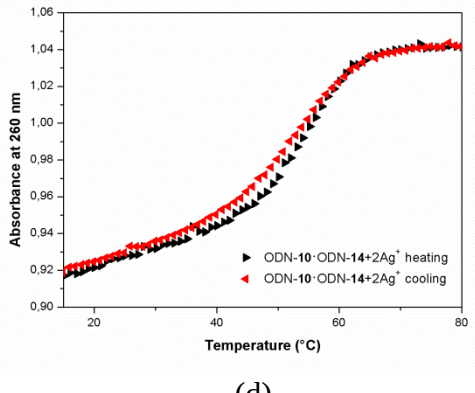
Absorbance at 260 nm
Temperature (°C)
ODN-10·ODN-14+2Ag+ heating
ODN-10·ODN-14+2Ag+ cooling

(d)

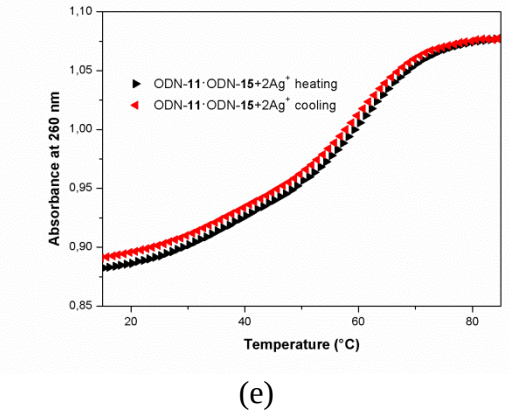
Absorbance at 260 nm
Temperature (°C)
ODN-11·ODN-15+2Ag+ heating
ODN-11·ODN-15+2Ag+ cooling

(e)

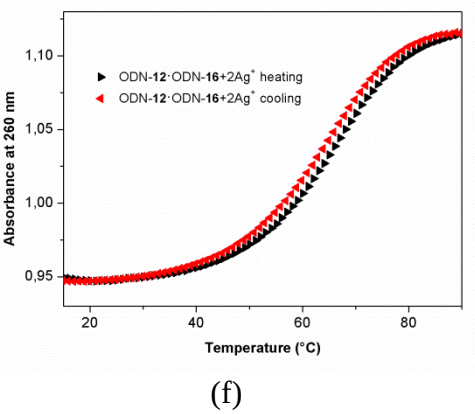
Absorbance at 260 nm
Temperature (°C)
ODN-12·ODN-16+2Ag+ heating
ODN-12·ODN-16+2Ag+ cooling

(f)

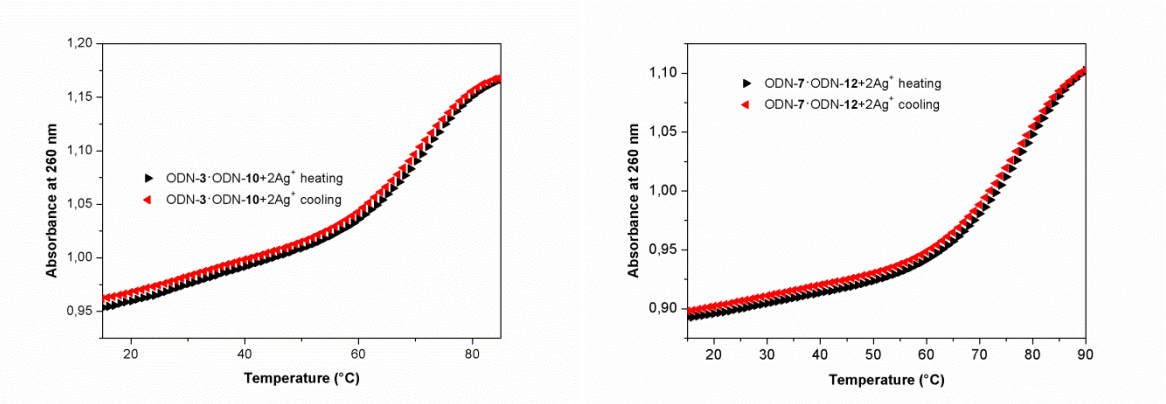

(g) (h)

Fig. 20A Thermal denaturation curves (heating and cooling) of ps and aps duplexes with increasing concentration of Ag^+ ions. The experiments were performed with 5 μM duplex concentration in 100 mM NaOAc, 10 mM $Mg(OAc)_2$ buffer (pH 7.5) at 260 nm. (a) ODN-**3** • ODN-**4**. (b) ODN-**5** • ODN-**6**. (c) ODN-**7** • ODN-**8**. (d) ODN-**10** • ODN-**14**. (e) ODN-**11** • ODN-**15**. (f) ODN-**12** • ODN-**16**. (g) ODN-**3** • ODN-**10**. (h) ODN-**7** • ODN-**12**.

References.

1 J. A. McDowell and D. H. Turner, *Biochemistry*, 1996, **35**, 14077−14089.

2 (*a*) D. Goldman and T. I. Kalman, *Nucleosides Nucleotides*, 1983, **2**, 175-187; (*b*) K. Gislason and S. T. Sigurdsson, *Eur. J. Org. Chem.*, 2010, 4713-4718.

3 A. T. R. Williams, S. A. Winfield and J. N. Miller, *Analyst*, 1983, **108**, 1067-1071.

4 (*a*) H. Torigoe, Y. Miyakawa, A. Ono and T. Kozasa, *Nucleosides, Nucleotides Nucleic Acids*, 2011, **30**, 149-167; (*b*) H. Torigoe, I. Okamoto, T. Dairaku, Y. Tanaka, A. Ono and T. Kozasa, *Biochimie*, 2012, **94**, 2431-2440.

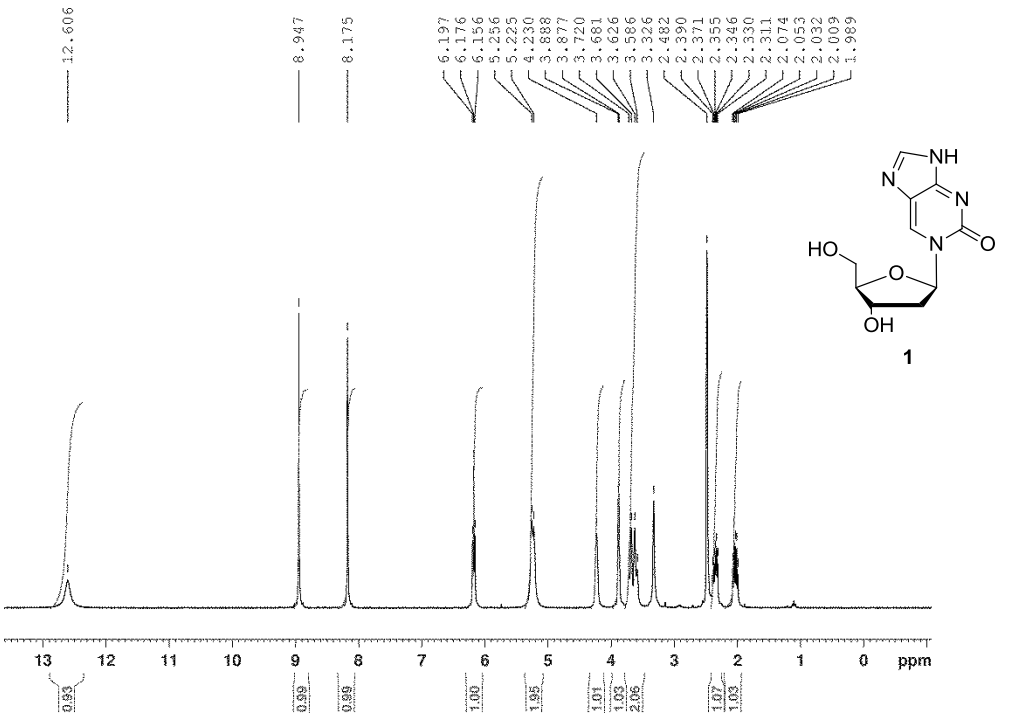

Fig. S21 ^{1}H NMR (300 MHz, DMSO-d_6) spectrum of compound **1**.

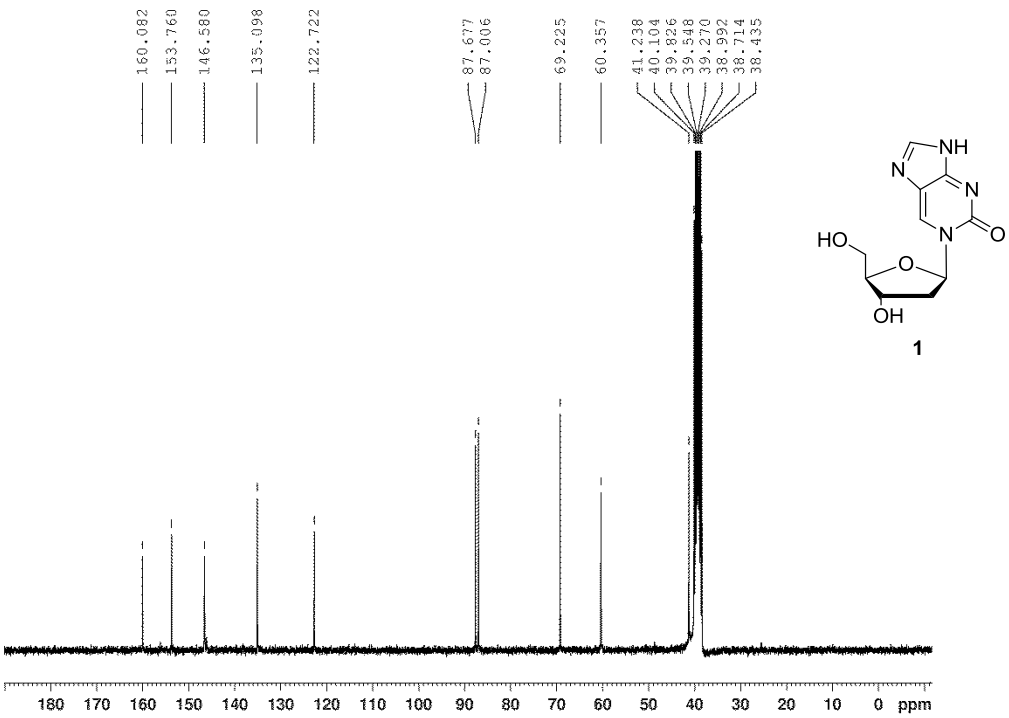

Fig. S22 ^{13}C NMR (75 MHz, DMSO-d_6) spectrum of compound **1**.

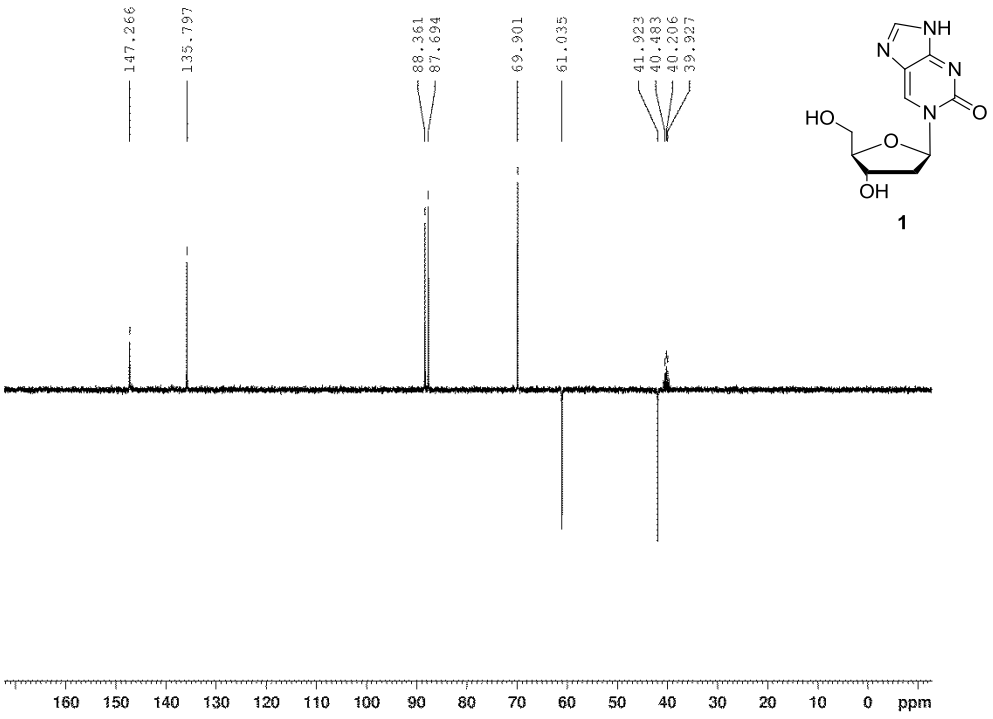

Fig. S23 DEPT-135 (75 MHz, DMSO-d_6) spectrum of compound **1**.

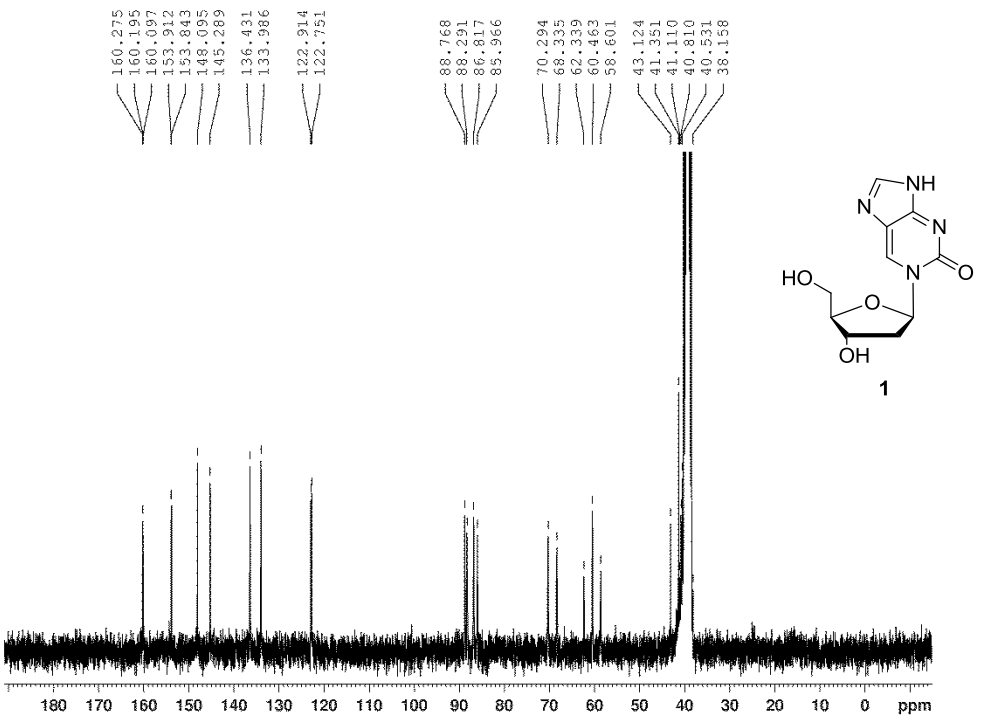

Fig. S24 ^{1}H-^{13}C gated-decoupled (75 MHz, DMSO-d_6) spectrum of compound **1**.

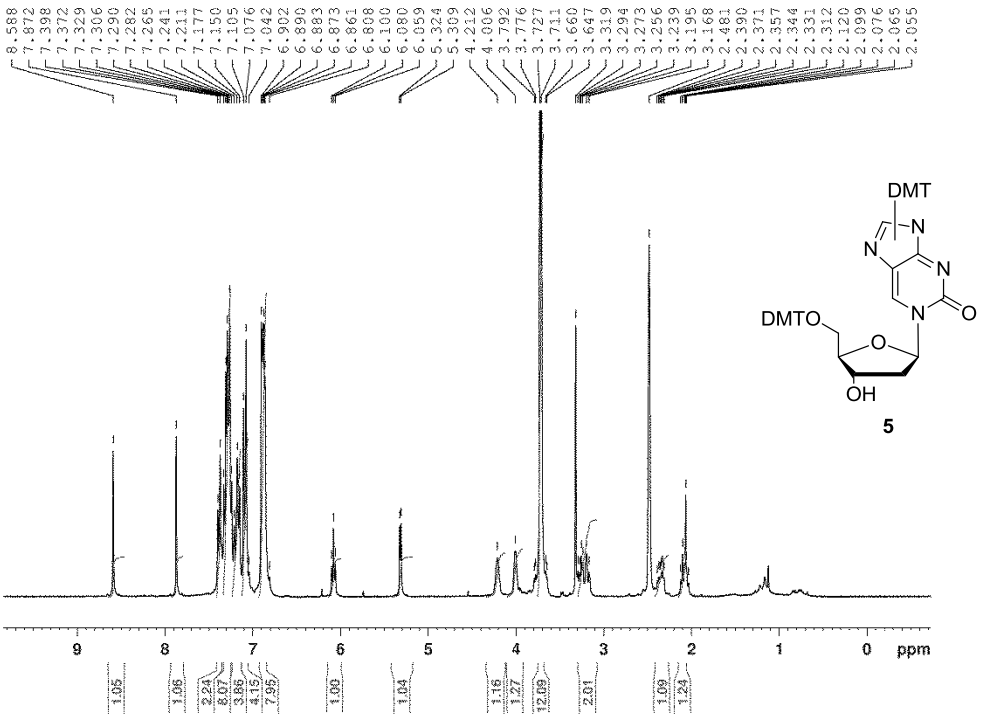

Fig. S25 ^{1}H NMR (300 MHz, DMSO-d_6) spectrum of compound **5**.

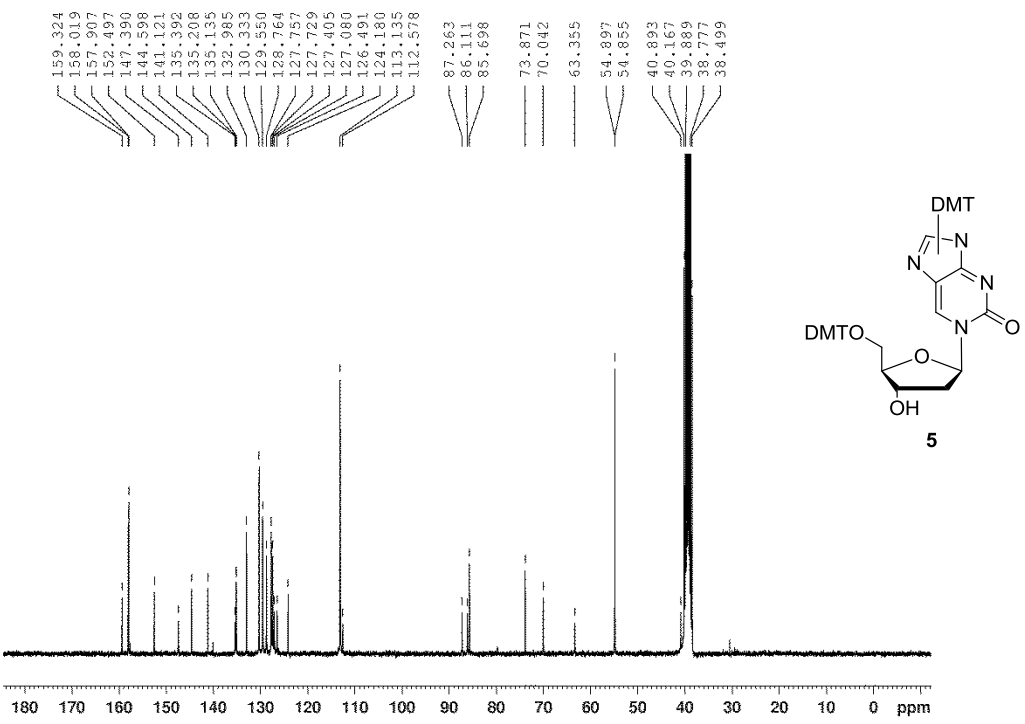

Fig. S26 ^{13}C NMR (75 MHz, DMSO-d_6) spectrum of compound **5**.

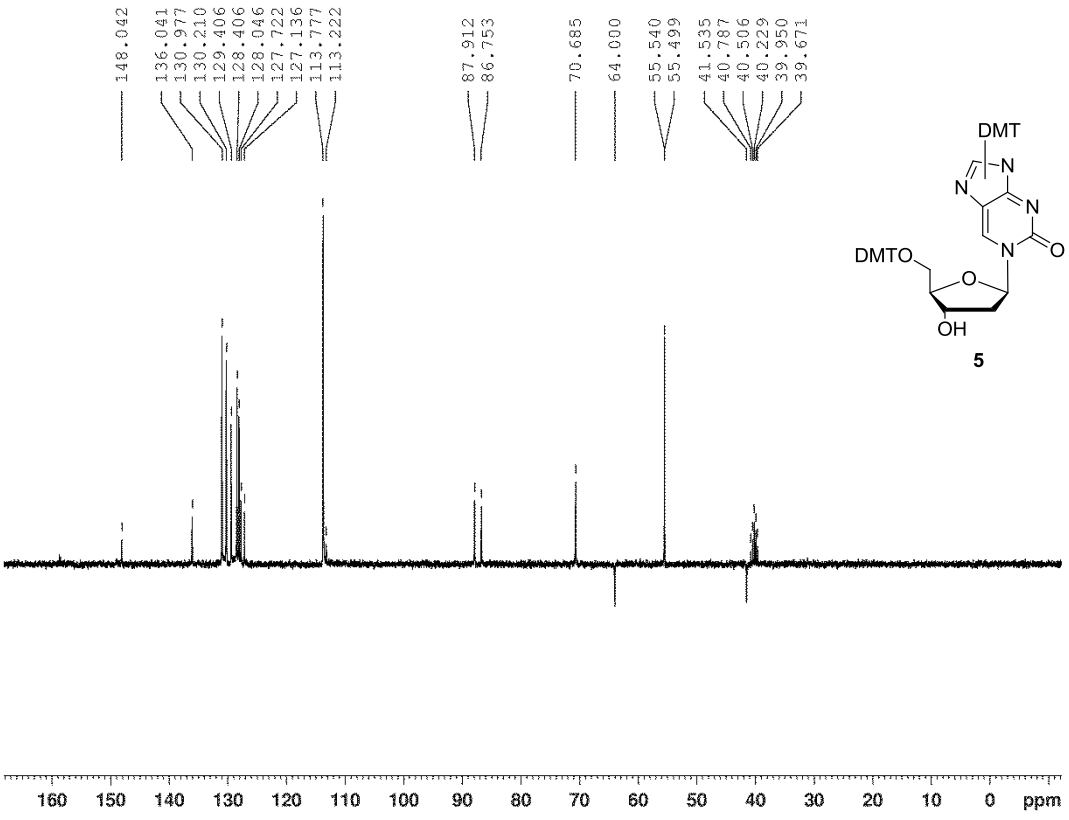

Fig. S27 DEPT-135 (75 MHz, DMSO-d_6) spectrum of compound **5**.

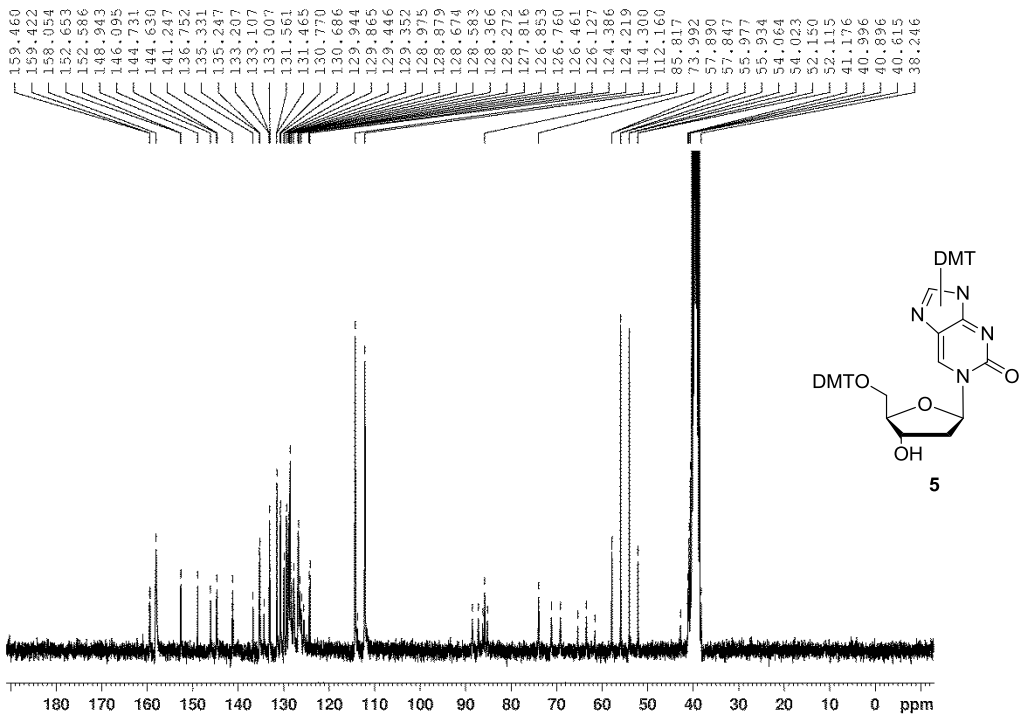

Fig. S28 ^{1}H-^{13}C gated-decoupled (75 MHz, DMSO-d_6) spectrum of compound **5**.

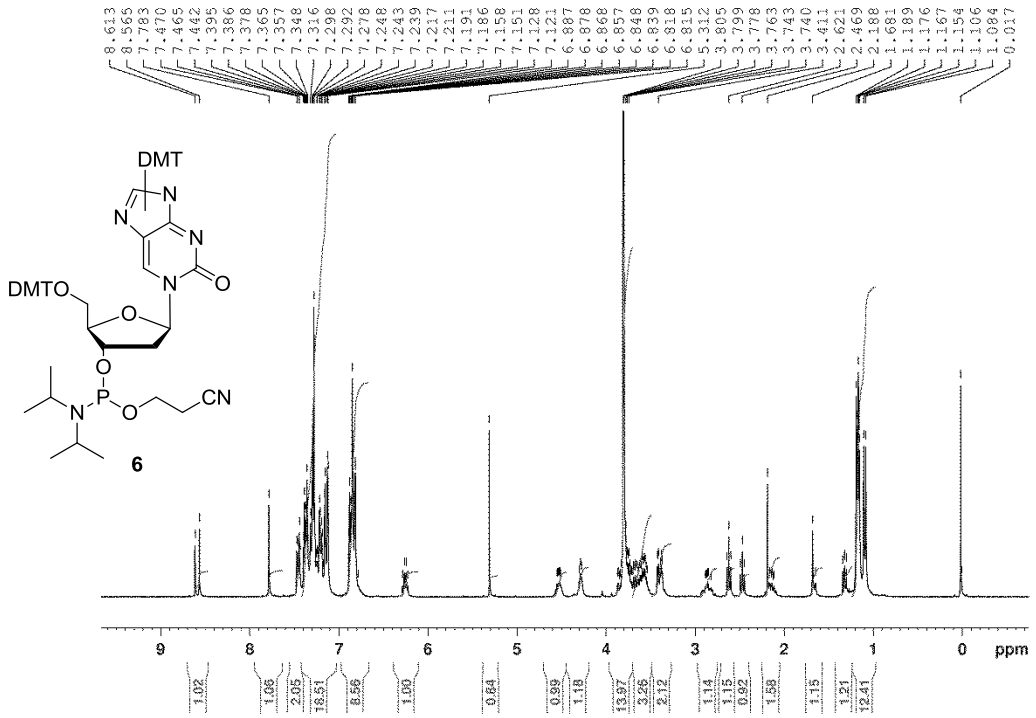

Fig. S29 ^{1}H NMR (300 MHz, $CDCl_3$) spectrum of compound **6**.

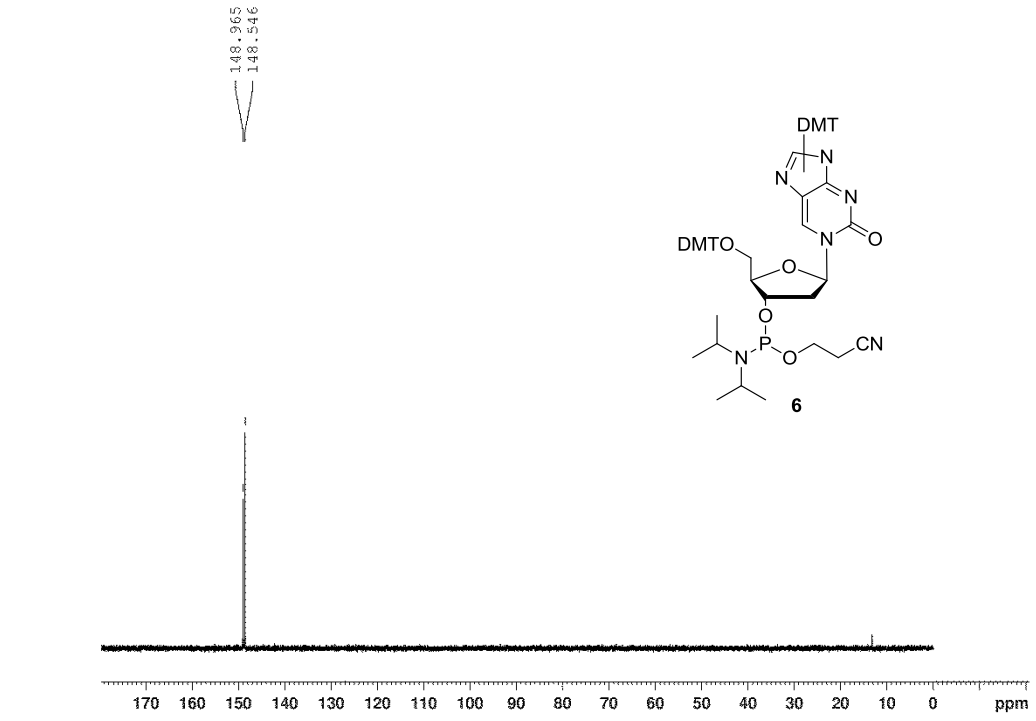

Fig. S30 ^{31}P NMR (121 MHz, $CDCl_3$) spectrum of compound **6**.

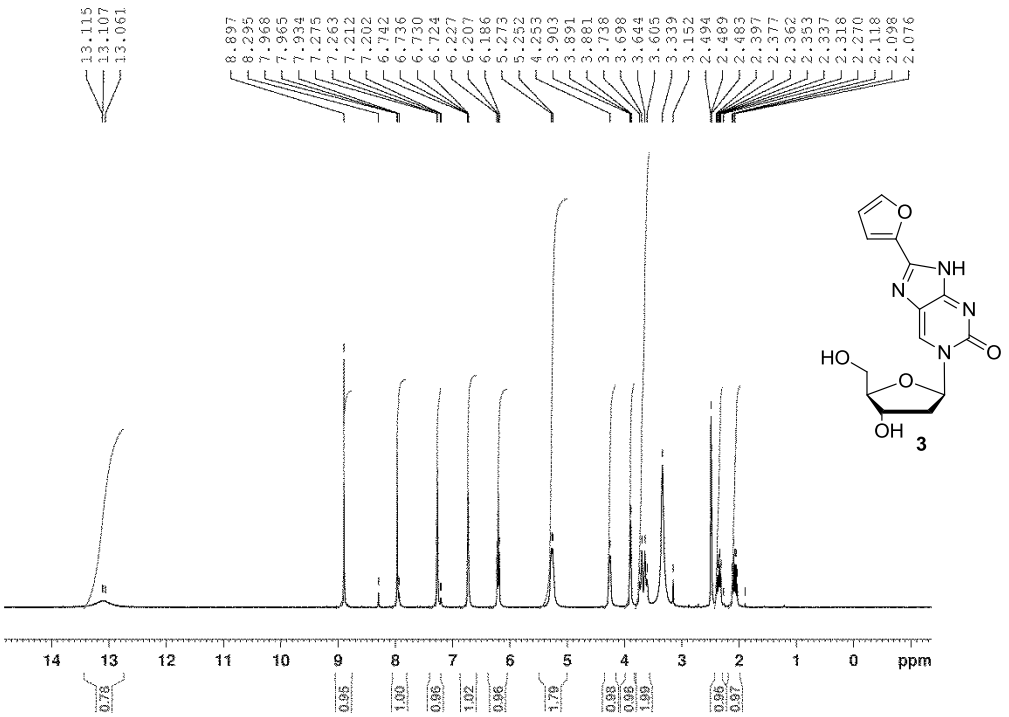

Fig. S31 ^{1}H NMR (300 MHz, DMSO-d_6) spectrum of compound **3**.

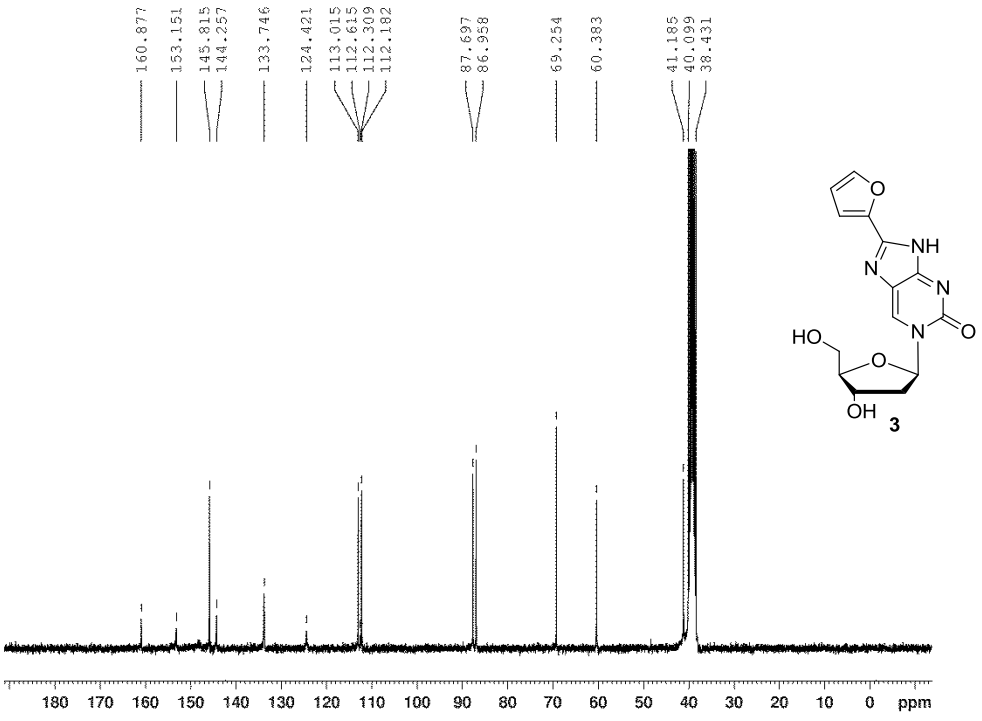

Fig. S32 ^{13}C NMR (75 MHz, DMSO-d_6) spectrum of compound **3**.

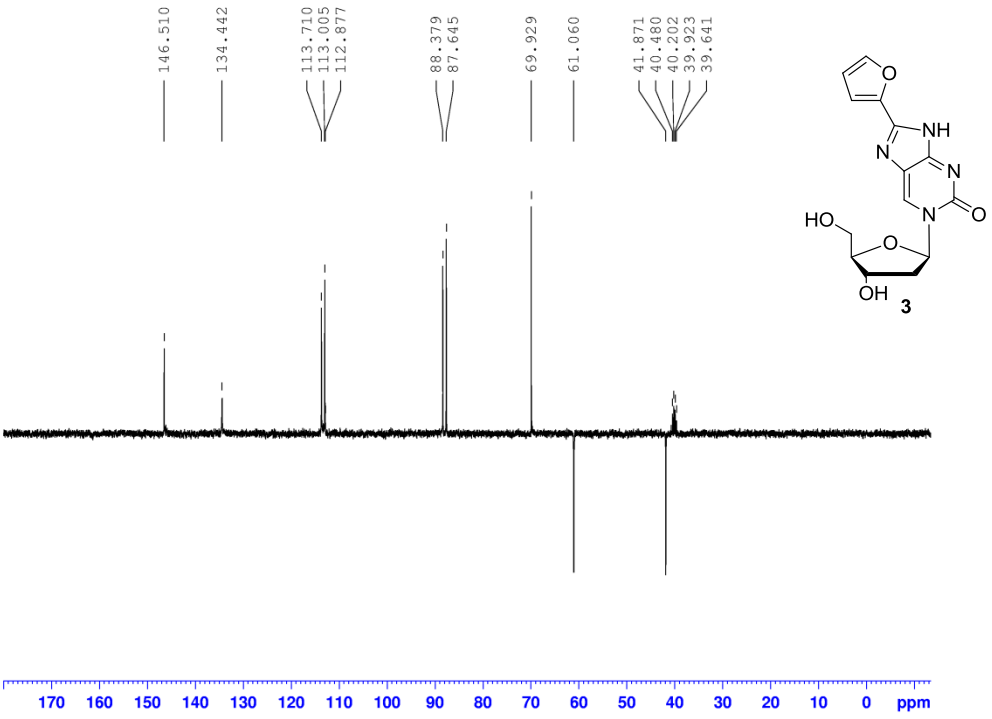

Fig. S33 DEPT-135 (75 MHz, DMSO-d_6) spectrum of compound **3**.

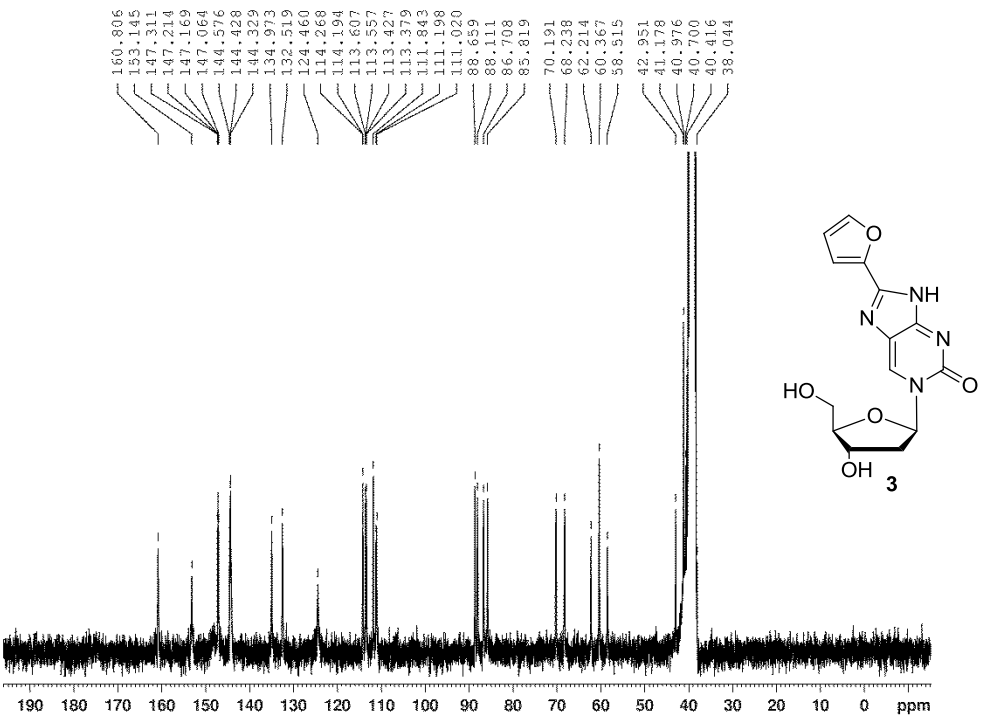

Fig. S34 ^{1}H-^{13}C gated-decoupled (75 MHz, DMSO-d_6) spectrum of compound **3**.

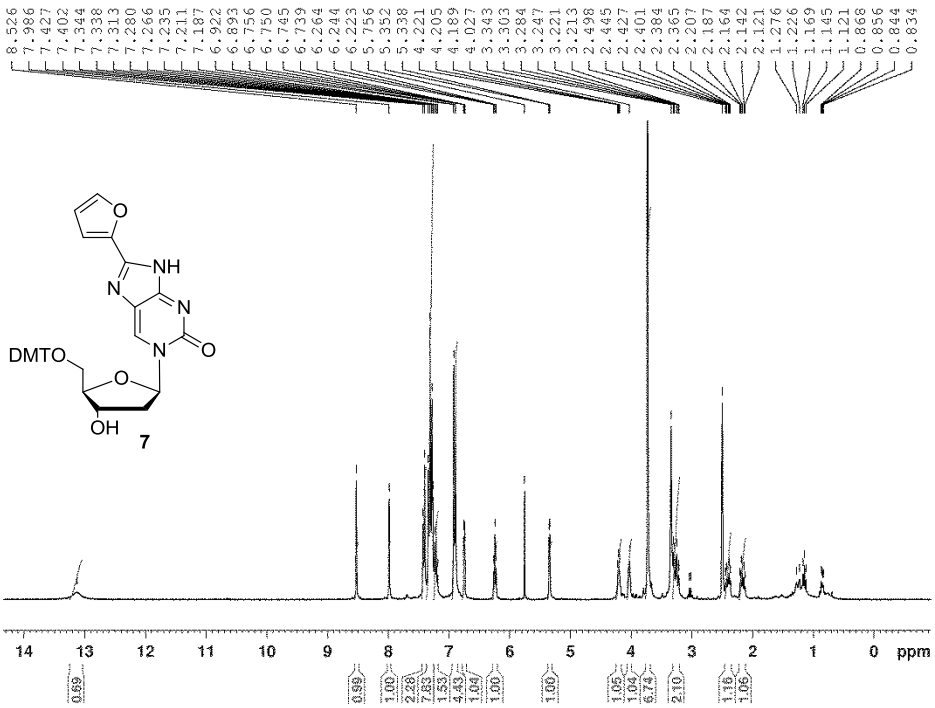

Fig. S35 ^{1}H NMR (300 MHz, DMSO-d_6) spectrum of compound **7**.

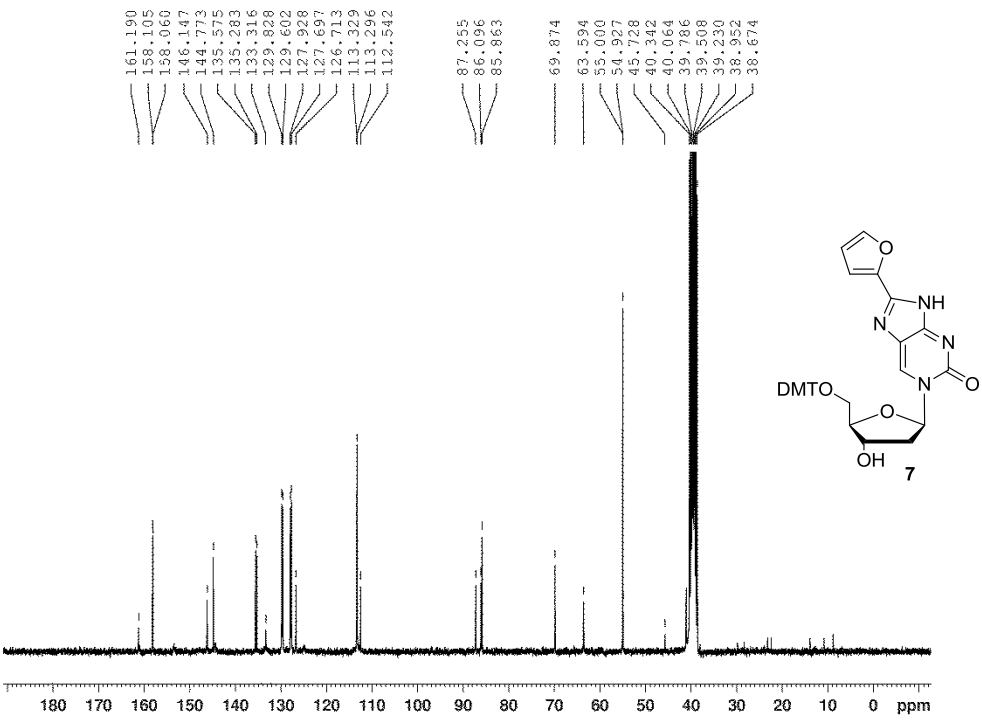

Fig. S36 ^{13}C NMR (75 MHz, DMSO-d_6) spectrum of compound **7**.

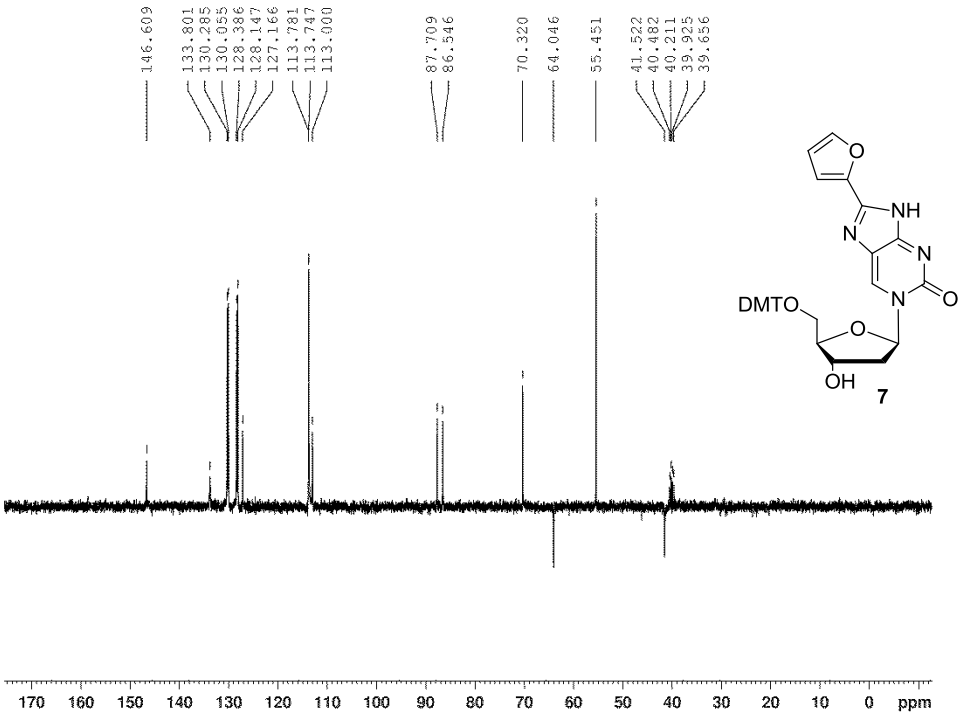

Fig. S37 DEPT-135 (75 MHz, DMSO-d_6) spectrum of compound **7**.

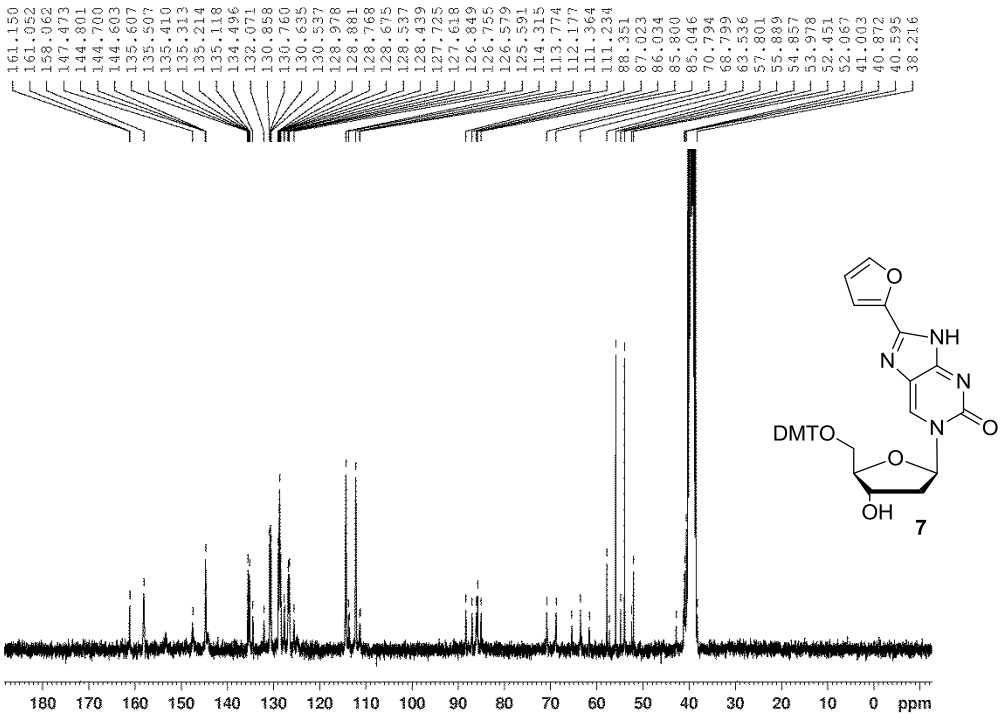

Fig. S38 ^{1}H-^{13}C gated-decoupled (75 MHz, DMSO-d_6) spectrum of compound **7**.

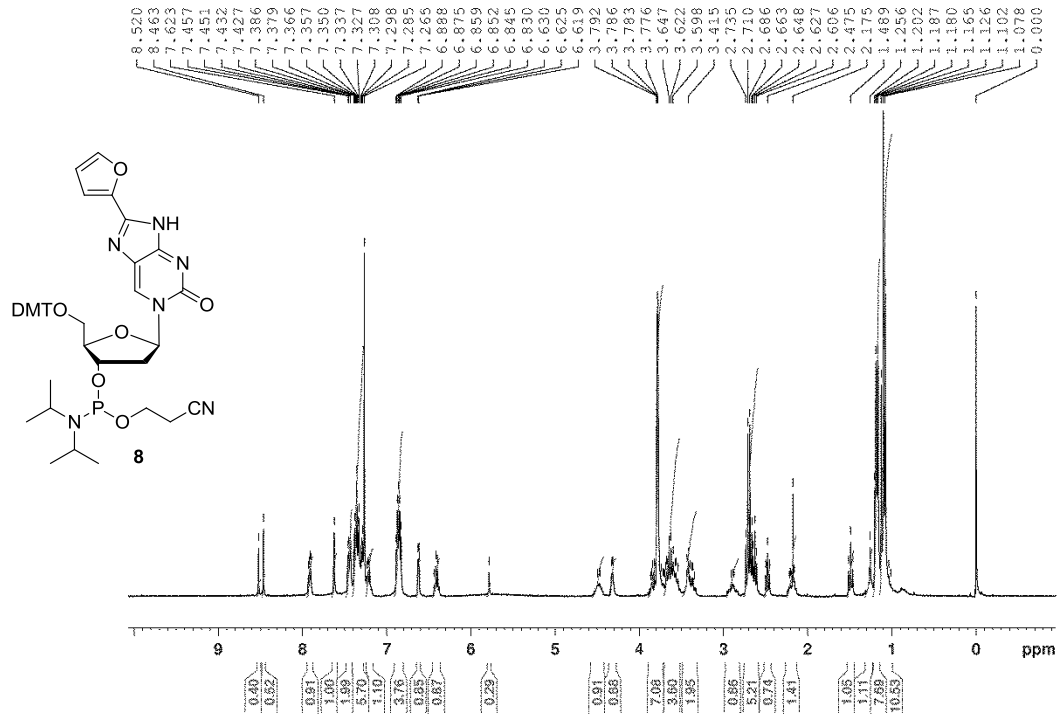

Fig. S39 ^{1}H NMR (300 MHz, $CDCl_3$) spectrum of compound **8**.

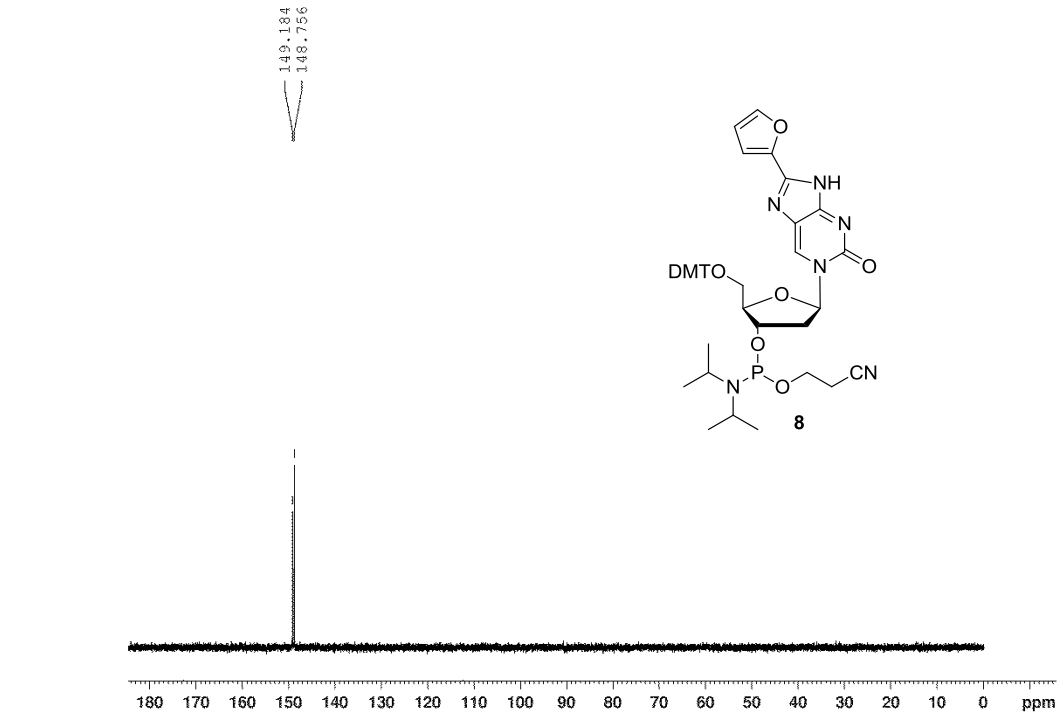

Fig. S40 ^{31}P NMR (121 MHz, $CDCl_3$) spectrum of compound **8**.